Biogeography of marine giant viruses reveals their interplay with eukaryotes and ecological functions

Hisashi Endo[1], Romain Blanc-Mathieu[1,2], Yanze Li[1], Guillem Salazar[3], Nicolas Henry[4,5], Karine Labadie[6], Colomban de Vargas[4,5], Matthew B. Sullivan[7,8], Chris Bowler[9,10], Patrick Wincker[10,11], Lee Karp-Boss[12], Shinichi Sunagawa[3], Hiroyuki Ogata[1,*]

Affiliations:

1. Bioinformatics Center, Institute for Chemical Research, Kyoto University, Gokasho, Uji, Kyoto, 611-0011, Japan
2. Laboratoire de Physiologie Cellulaire & Végétale, CEA, Univ. Grenoble Alpes, CNRS, INRA, IRIG, Grenoble, France
3. Department of Biology, Institute of Microbiology and Swiss Institute of Bioinformatics, ETH Zürich, Zürich 8093, Switzerland
4. CNRS, UMR 7144, Station Biologique de Roscoff, Place Georges Teissier, 29680 Roscoff, France.
5. Sorbonne Universités, UPMC Université Paris 06, UMR 7144, Station Biologique de Roscoff, Place Georges Teissier, 29680 Roscoff, France.
6. Genoscope, Institut de Biologie François-Jacob, Commissariat à l'Énergie Atomique (CEA), Université Paris-Saclay, Évry, France.
7. Department of Microbiology, The Ohio State University, Columbus, OH 43210, USA
8. Department of Civil, Environmental and Geodetic Engineering, The Ohio State University, Columbus, OH 43210, USA
9. Institut de Biologie de l'ENS (IBENS), Département de biologie, École normale supérieure, CNRS, INSERM, Université PSL, Paris 75005, France
10. Research Federation for the study of Global Ocean Systems Ecology and Evolution, FR2022/Tara Oceans GOSEE, 3 rue Michel-Ange, 75016 Paris, France
11. Génomique Métabolique, Genoscope, Institut de Biologie François Jacob, Commissariat à l'Énergie Atomique (CEA), CNRS, Université Évry, Université Paris-Saclay, Évry, France.

12. School of Marine Sciences, University of Maine, Orono, ME, USA

Corresponding author:

H. Ogata, E-mail: ogata@kuicr. kyoto-u.ac.jp, Phone: +81-774-38-3270

Abstract

Nucleocytoplasmic large DNA viruses (NCLDVs) are ubiquitous in marine environments and infect diverse eukaryotes. However, little is known about their biogeography and ecology in the ocean. By leveraging the *Tara* Oceans pole-to-pole metagenomic data set, we investigated the distribution of NCLDVs across size fractions, depths and biomes, as well as their associations with eukaryotic communities. Our analyses revealed a heterogeneous distribution of NCLDVs across oceans, with an elevated uniqueness in polar biomes. The community structures of NCLDV families were correlated with specific eukaryotic lineages including many photosynthetic groups. NCDLV communities were generally distinct between surface and mesopelagic zones, but at some locations, they exhibited a high similarity between the two depths. This vertical similarity was correlated to surface phytoplankton biomass but not to physical mixing processes, suggesting the potential role of vertical export in structuring mesopelagic NCLDV communities. These results underscore the importance of the coupling between NCLDVs and eukaryotes in biogeochemical processes in the ocean.

Introduction

The photic zone is the most productive layer of the ocean, containing a wide variety of microorganisms such as bacteria, autotrophic and heterotrophic protists and multicellular organisms. The population dynamics of these organisms determine the flows of energy and materials through marine food webs, playing a fundamental role in ecosystem functioning and biogeochemical cycles in the ocean[1,2]. Viruses exert a top-down control on marine organisms and release material to the pools of particulate and dissolved organic matter[3]. This material and remineralized inorganic nutrients are utilized by autotrophic and mixotrophic phytoplankton[4]. The recycling of nutrients in the surface layer potentially reduces the transfer of fixed organic carbon to higher trophic levels and the deep sea[5,6]. However, it is also possible that viruses enhance downward carbon flux by facilitating cell aggregation and producing carbon-enriched materials from infected cells[7-9].

Nucleocytoplasmic large DNA viruses (NCLDVs or so-called "giant viruses") represent a monophyletic group of viruses that infect a variety of eukaryotic lineages[10-12]. Studies focusing on conserved marker genes such as family B DNA polymerase (*polB*) have revealed that NCLDVs are highly diverse and abundant in aquatic environments[13-16]. The diversity of a family of NCLDVs, namely *Mimiviridae*, exceeds that of bacteria and archaea in the ocean[17] and their richness in a few liters of seawater can reach more than 5,000 operational taxonomic units[18]. More recently, several thousand draft genomes (i.e., metagenome-assembled genomes; MAGs) of NCLDVs were constructed from environmental sequences, thanks to the development of high-throughput sequencing and bioinformatics technologies[19,20]. However, the global biogeography of marine NCLDVs still remains under-explored.

A growing number of marine eukaryotes have been reported as host organisms of NCLDVs, particularly phytoplankton groups such as haptophytes, chlorophytes and dinoflagellates[21-23]. Other eukaryotic lineages, including non-photosynthetic organisms such as bicosoecids and choanoflagellates, have also been reported as host organisms of

NCLDVs in marine environments[24,25]. These studies collectively suggest the ecological importance of NCLDVs in the ocean via top-down effects on eukaryotic communities. However, our knowledge of NCLDV-host relationships is highly limited, given the large phylogenetic diversities of NCLDVs and microeukaryotes.

Here we reveal patterns in the global biogeography of NCLDVs using the metagenomic data from the *Tara* Oceans project. The metagenomic data cover varying geographic regions including polar and deep-sea ecosystems, in which NCLDVs are under-researched[26-28]. We constructed NCLDV taxonomic abundance profiles for 283 samples, representing two viral size fractions, three ocean depth ranges (surface, deep chlorophyll maximum and mesopelagic), and four biomes (coastal, trades, westerlies and polar). The global biogeography of NCLDVs derived from these data reveals strong associations between NCLDVs and eukaryotic microorganisms. Furthermore, vertical connectivity of NCLDV communities indicates a possible mechanism for how mesopelagic NCLDV communities are structured with respect to ocean biogeochemical processes.

Results

NCLDV phylotypes detected in *Tara* Oceans metagenomes

We detected 6,818 PolBs affiliated with NCLDVs in the second version of the Ocean Microbial Reference Gene Catalog (OM-RGC.v2)[28] using the pplacer phylogenetic placement method[29] (see methods for details). The OM-RGC.v2 was built based on 370 *Tara* Oceans metagenomes from femto- (<0.2 μm; 151 samples), pico- (0.22–1.6 or 0.22–3.0 μm; 180 samples) and other (39 samples) size fractions. After removing 32 samples with a low NCLDV frequency and 55 samples from non-target size fractions and depths, the remaining 283 samples contained 6,783 NCLDV PolB sequences. The pplacer classified these PolBs into nine NCLDV families/lineages. The number of phylotypes (distinct *polB* at 95% nucleotide sequence identity) was the largest in *Mimiviridae* (5,091 phylotypes), followed by *Phycodnaviridae* (981 phylotypes). The

number of phylotypes taxonomically assigned to *Iridoviridae*, *Medusavirus* and *Asfarviridae*, were 239, 120 and 109, respectively. We also detected PolBs assigned to *Pithoviridae* (93), *Ascoviridae* (78), *Poxviridae* (51) and *Marseilleviridae* (21). However, *Poxviridae* was omitted from our discussion as the environmental gene sequences were distantly related to known *Poxviridae*. Rarefaction analysis showed that, at the end of sampling, the number of NCLDV phylotypes increased by less than 0.01% per sample for all samples, and ranged from 0.02% to 0.32% when samples were divided into different size fractions, depths and biomes (Extended Data Fig. 1).

To examine detailed phylogenetic affiliation and to visualize the dispersal characteristics of each NCLDV phylotypes detected by pplacer, we constructed a phylogenetic tree using selected PolB sequences (Extended Data Figs. 2–4). Among the *Mimiviridae* family, genes closely related to the algal-infecting subfamily, recently proposed as "Mesomimivirinae" (e.g., AaV, CeV, pkV, PgV, PoV and TetV)[30], which infect pelagophytes (the genus *Aureococcus*), haptophytes (the genera *Haptolina*, *Prymnesium* and *Phaeocystis*), and chlorophytes (the genera *Pyramimonas* and *Tetraselmis*), were relatively abundant. On the other hand, only a few sequences were affiliated with the subfamilies "Megamimivirinae" and "Klosneuvirinae" except the *Cafeteria roenbergensis virus* (CroV), which is the only member of "Megamimivirinae" isolated from the marine environment[24]. Among *Phycodnaviridae*, the genus *Prasinovirus* (e.g., BpV, MpV, OtV and OlV), which infect chlorophyte genera such as *Bathycoccus*, *Micromonas* and *Ostreococcus*, showed the highest richness.

Heterogeneity in NCLDV community structure across size, depth and biomes

The dominant NCLDV taxa detected from all sample locations and depths in the pico-size fraction were *Mimiviridae* and *Phycodnaviridae*, with average contributions of 64.6% and 25.4%, respectively (Fig. 1A). The dominant groups of NCLDVs varied widely among sites and depths in samples from the femto-size fraction (Fig. 1B). In this fraction, *Phycodnaviridae* and *Asfarviridae* had relatively high contributions to the total

NCLDVs with the mean values of 29.7% and 19.9%, respectively. *Mimiviridae* and *Ascoviridae* were also important contributors with mean values of 12.2% and 11.1%, respectively.

A non-metric multidimensional scaling (NMDS) analysis showed that NCLDV assemblages clustered according to size fraction, depth and biome (Fig. 2A–2C). Significant differences in NCLDV community composition were detected among all categories (PERMANOVA, p <0.01), and size fraction, depth and biome explained 5.5%, 4.3% and 10.9% of the total variance, respectively.

Taxonomic richness (i.e., number of phylotypes) and Shannon's diversity index were used to investigate variation in NCLDV community diversity. In this study, we analyzed the samples from all depths and size fractions to compare diversity differences among depth ranges, although latitudinal trend in Shannon's diversity for pico-sized communities from the surface was reported previously[31]. In the pico-size fraction, mean values for NCLDV richness at the surface and in the DCM layer were about 1.7 times higher than that in the mesopelagic layer (Kruskal-Wallis and Dunn's post hoc test, p <0.01) (Extended Data Fig. 5A). In the femto-size fraction, NCLDV richness was significantly higher at the surface and MES layer than in the DCM layer (Dunn's test, p = 0.04–0.05), although the differences were small and not consistent with the pico-size fraction.

High uniqueness of NCLDV phylotypes in the Arctic Ocean

We analyzed the overlap and uniqueness of NCLDV phylotypes across different ecological zones (i.e., size fraction, depth and biome) to evaluate their ability to disperse across different environments. Each ecological category was divided into two major groups (i.e., pico- and femto-sizes, euphotic and mesopelagic zones, and polar and non-polar biomes), because the NCLDV community in mesopelagic zone or polar biome was separated most significantly from other depths or biomes (Fig. 2). We found 4,003 (59.0% to the total NCLDVs) shared NCLDV phylotypes across size fractions,

4,737 (69.8%) shared phylotypes across depth ranges, and 1,950 (28.7%) shared phylotypes across biomes (Fig. 3A). Only twelve unique phylotypes were detected in the femto-size fraction, whereas 2,768 unique phylotypes were identified in the pico-size fraction. The euphotic zone (surface and DCM) harbored 1,986 unique phylotypes, whereas the aphotic mesopelagic zone had only 60 unique phylotypes. The polar biome (the Arctic and the Southern Ocean) included 620 unique NCLDV phylotypes, whereas 4,213 unique NCLDVs were detected in non-polar biomes (i.e., trades, westerlies and coastal).

To further characterize regional differences in the NCLDV community, we investigated the total and unique NCLDV phylotypes observed in nine geographic regions and the phylotypes shared among regions. The total number of phylotypes was relatively high in the Atlantic, Pacific and Indian Oceans and in the Mediterranean Sea, with values of between 3,665 and 4,685 (Fig. 3B). Lower numbers of NCLDV phylotypes were identified from the Red Sea (2,653) and the Arctic Ocean (2,467). The Southern Ocean presented the lowest number of NCLDV phylotypes (561), although this was based on only 5 samples. The Arctic Ocean samples displayed a high number of unique NCLDV phylotypes (551), which corresponded to 22.3% of the total phylotypes detected in this region. In contrast, the number of unique phylotypes from other regions ranged from 0 to 134 (0.0% to 3.4%).

There was no linear or saturation trend in the number of total or unique NCLDV phylotypes with increasing sample size (Fig. 3C). The high proportion of unique phylotypes in the Arctic Ocean was not a function of sample size, although the number of total phylotypes detected in the Southern Ocean may be limited by the low number of samples. The phylogenetic positions of unique NCLDVs from the polar biome were dispersed across most of the NCLDV families (Fig. 4)

NCLDV distributions correlate with eukaryotic communities

A partial Mantel test was conducted to assess community associations among the

NCLDV families/lineages and major eukaryotic lineages. The pairwise partial correlation coefficients (Spearman's ρ) varied from –0.17 to 0.76 (Fig. 5A), and 93.6% of the examined pairs (225 out of 234 for the pico-size fraction and 213 out of 234 for the femto-size fraction) showed statistically significant correlations (p <0.01, permutation test) after false discovery rate (FDR) correction. Pairs from pico-sized NCLDV communities with a correlation coefficient ≥0.53 were considered to represent strong positive associations, because 8 out of 9 known marine virus-host lineage associations were recovered by this criterion (Figs. 5A and 5B). Using this threshold, 30 out of 234 NCLDV-eukaryote lineage pairs were found to have strong linkages (Fig. 5C). The NCLDV families/lineages were generally highly correlated with the known host groups among autotrophic and mixotrophic microalgae (haptophytes, chlorophytes, dinophytes, pelagophytes and raphidophytes) (ρ = 0.54–0.67). Interestingly, *Mimiviridae* was strongly correlated with chrysophyte microalgae (ρ = 0.65), which are not currently known as NCLDV hosts. Other than algal lineages, a strong positive correlation was found between *Mimiviridae* and heterotrophic eukaryote choanoflagellates (ρ = 0.76), which are a known lineage of *Mimiviridae*. A group of non-photosynthetic heterokonts bicosoecids are also a known host of the *Mimiviridae* species CroV in marine environments, but this group was not highly correlated with *Mimiviridae* (ρ = 0.30).

Potential chrysophyte viruses constitute novel clades of *Mimiviridae*

To explore possible associations between NCLDVs and chrysophytes as indicated by the Mantel's regression analysis (Fig. 5C), we tested for chrysophyte-derived genes in the metagenome-assembled genomes (MAGs) of NCLDVs generated by Schultz et al. (2020)[19] and Moniruzzaman et al. (2020)[20]. The results showed that 89 (82 after removing redundancy) out of 2,263 MAGs contained genes closely related to the transcripts of the chrysophytes (Supplementary Data 1). Comparisons between PolB sequences revealed 27 PolBs from the OM-RGC.v2 that were closely related to the

NCLDV MAGs with chrysophyte homologs. Most of these PolBs constituted novel clades within the branches of *Mimiviridae* (Fig. 4; Extended Data Fig. 4). We confirmed that other genes in the contigs that contained chrysophyte homologs are highly similar to the *Mimiviridae* or *Phycodnaviridae* sequences in many cases (Extended Data Fig. 6).

Vertical connectivity of NCLDV communities

The vertical connectivity of NCLDV communities was investigated using Bray-Curtis community similarity measures to compare between epipelagic (surface or DCM) and mesopelagic samples at individual sampling locations. The Bray-Curtis similarities were less than 0.10 for about half of the tested locations (20 out of 36 surface sites and 13 out of 26 DCM sites; Fig. 6A; Extended Data Fig. 7A). All sites in the Arctic Ocean and several sites in tropical and subtropical regions showed relatively high similarities between the two depth (0.15 to 0.60). The NCLDV community similarity value was positively correlated with the chlorophyll *a* concentration in the epipelagic layer (Spearman's $\rho = 0.52$, $p < 0.01$, asymptotic t approximation, n = 36 for surface; $\rho = 0.44$, $p = 0.02$, n = 25 for DCM) and NCLDV richness in the mesopelagic layer ($\rho = 0.82$, $p < 0.01$, n = 36 for surface; $\rho = 0.70$, $p < 0.01$, n = 26 for DCM) (Figs. 6B and 6C; Extended Data Figs. 7B and 7C). We also evaluated relationships between NCLDV vertical similarity and physical environmental factors including: the sampling depth of mesopelagic water, the mixed layer depth, and the temperature difference between epipelagic and mesopelagic waters. No significant correlations were detected among these parameters ($p > 0.05$, n = 32–36 for surface samples and n = 25–26 for DCM samples) (Figs. 6D–F; Extended Data Figs. 7D–F).

We plotted correlations among the relative contributions of NCLDV phylotypes between the euphotic and aphotic zones at all sampling locations (Extended Data Figs. 8 and 9). Where there was a strong similarity in the NCLDV community found at different depths, *Phycodnaviridae* generally contributed highly to samples from the

Arctic Ocean (e.g., TARA stations 158, 201 and 209), and both *Mimiviridae* and *Phycodnaviridae* contributed strongly in tropical and subtropical regions (e.g., stations 72, 110 and 122).

Discussion

We investigated the diversity and community structure of NCLDVs based on metagenomic PolB sequences collected from the world oceans. NCLDV communities differed substantially between pico- and femto- size fractions (Fig. 1). NCLDV communities in the pico-size fractions were dominated by *Mimiviridae* and *Phycodnaviridae*, regardless of sampling location or depth (Fig. 1A). In marine environments, species from the haptophytes (the genera *Prymnesium*, *Haptolina*, and *Phaeocystis*), chlorophytes (*Pyramimonas*), pelagophytes (*Aureococcus*), bicosoecids (*Cafeteria*) and choanoflagellates (*Bicosta*) are known hosts of *Mimiviridae*, while species of haptophytes (*Emiliania*), chlorophytes (*Ostreococcus*, *Micromonas* and *Bathycoccus*) and raphidophytes (*Heterosigma*) have been reported as *Phycodnaviridae* hosts (Virus-Host DB)[32]. Although the dominance of *Mimiviridae* and *Phycodnaviridae* have been reported in previous studies, mainly from coastal seawater[13,14], our results demonstrate the ubiquitous nature of these protist-infecting viruses across world ocean biomes. It is worth noting that most of the NCLDVs (99.7%) detected from the femto-size fraction were also present in the pico-size fraction (Fig. 3A), despite the large differences in relative abundance between two size fractions at each location. Therefore, the abundance information can be important for characterizing the differences of NCLDV communities. A proportion of the NCLDVs in the pico-size fraction were present within infected cells, because cell sizes of some host species such as *Aureococcus anophagefferens* and *Micromonas pusilla* are less than 3 μm. Thus, the abundance of these lineages in the pico-size fraction may be partly enriched by the viruses replicating inside their hosts.

In addition to *Phycodnaviridae* and *Mimiviridae*, *Asfarviridae* also contribute an

278 important proportion of NCLDVs in the femto-size fraction of most euphotic zones (Fig.
279 1B). Although very limited information is available regarding the natural hosts for this
280 group, a representative *Asfarviridae*-like species in marine environments is *Heterocapsa*
281 *circularisquama* DNA virus (HcDNAV), which infects the red-tide-forming
282 dinoflagellate *H. circularisquama*[33]. In the terrestrial ecosystem, this viral family is
283 known to infect a wide variety of organisms such as amoebozoa, arthropods and
284 mammals[32,34]. Given the broad range of host species for this viral lineage, there may be
285 an unknown but wide-spread host taxa for *Asfarviridae* in the ocean.
286 Our study revealed a heterogeneous pattern in the distribution of NCLDVs across the
287 oceans of the world (Fig. 2C). Although there are limited studies available on the factors
288 controlling the large-scale distribution of viruses, it is widely accepted that both
289 deterministic (environmental factors and inter-specific interactions) and stochastic
290 processes (e.g., immigration and speciation) are important in making up microbial
291 assemblages[35-37]. The distribution and diversity of viruses would not be directly affected
292 by environmental variables such as temperature and nutrient availability, but is directly
293 influenced by the geographic ranges of their host species[3,38]. Recent work with
294 cyanophages demonstrated that a significant number of free-living viruses are locally
295 produced through active infection rather than from migration[39]. Therefore, we expect
296 that viral community structure will reflect host distribution as well as infectious activity.
297 Despite significant differences in community composition across oceanic biomes, we
298 found that most NCLDV phylotypes are dispersed throughout tropical and temperate
299 regions (Figs. 3A and 3B), presumably following their host community composition,
300 which is primarily determined by temperature[40]. However, the polar biome (mainly the
301 Arctic Ocean) constitutes a "hotspot" of unique NCLDV phylotypes from a wide
302 variety of families, despite having a low total richness in comparison to other regions
303 (Figs. 3B and 3C). We revealed that NCLDVs unique to non-polar biome were also
304 abundant (Fig. 4), indicating a strong separation of NCLDV communities between polar
305 and non-polar biomes. A geographical barrier and steep environmental gradients may

306 underlie this distinct ecosystem structure (i.e., different host communities and their
307 productivity) in the Arctic Ocean[27,28,31]. Moreover, the Arctic Ocean is characterized by
308 high amounts of river discharge, contributing more than 10% to global runoff flux[41].
309 Consequently, biological processes in the Arctic may be influenced by river inputs from
310 terrestrial ecosystems. These factors may collectively contribute to the remarkable
311 number of unique NCLDV phylotypes found in the Arctic, that were undetectable in
312 other regions. The biogeography of NCLDVs on a global scale implies a tight link
313 between the NCLDVs and the distribution of their hosts, which is strongly influenced
314 by physicochemical and biological factors.

315 Tight coupling between NCLDVs and their hosts was further corroborated by our
316 partial Mantel statistics, which described both known virus-host interactions and
317 additional but currently unrecognized associations between viruses and eukaryotic
318 lineages at the community level. Using the pico-sized NCLDV community, we detected
319 almost all known virus-host interactions, except for those involving Bicoecea (Fig. 5C).
320 This demonstrates that distance-based correlation analysis using global ocean samples is
321 useful for detecting virus-host interplay in natural environments, although the
322 validations of the previously unknown associations remain to be further explored.
323 Strong positive relationships between NCLDVs and eukaryotes involved many
324 phytoplankton lineages including haptophytes, chlorophytes, dinophytes, pelagophytes
325 and raphidophytes, all of which include known host lineages of NCLDVs (Fig. 5C).
326 Strong correlations were also detected with heterotrophic choanoflagellates, which have
327 recently been identified as a novel host of *Mimiviridae*[25]. Some NCLDVs, especially
328 *Mimiviridae*, had strong correlations with chrysophytes, although no host species have
329 yet been reported for this lineage. Many environmental NCLDV genomes were found to
330 encode genes that are likely to be derived from marine chrysophytes (Supplementary
331 Data 1–3). Taxonomic analyses based on PolB phylogeny and homology search
332 revealed that most of these phylotypes represent previously unknown clades of the
333 *Mimiviridae* tree (Extended Data 4 and 6; Supplementary Data 4), suggesting that

334 chrysophytes may be an important host lineage of *Mimiviridae* in the ocean.

335 The global distribution of NCLDVs are determined by the geographic ranges of their
336 host organisms. Therefore, the virus-eukaryote associations that we detected likely arose
337 under these constraints. On the other hand, it is expected that NCLDVs influence the
338 abundance of eukaryotes at a local scale. Previous studies show that bacterial viruses
339 have an important role in determining bacterial mortality, because they substantially
340 outnumber their hosts and have highly specific infection mechanisms[42]. Similarly,
341 NCLDVs are reported to be more abundant than their host cells and have high infection
342 specificity[11,14,43]. For example, *Emiliania huxleyi* viruses (EhVs) of the
343 *Phycodnaviridae* family are responsible for almost all of the mortality of the haptophyte
344 *E. huxleyi* during blooms[22,44,45]. Another field study suggests that viral lysis can explain
345 a greater proportion of phytoplankton mortality than grazing by zooplankton[6]. These
346 studies, combined with the global associations that were detected in this study,
347 emphasize the potential importance of NCLDVs in structuring eukaryotic communities.

348 Our results indicate that marine phytoplankton lineages could represent one of the
349 most important host groups of NCLDVs. Therefore, NCLDVs could be involved in the
350 regulation of biogeochemical processes mediated by phytoplankton. We investigated
351 this by assessing the vertical connectivity of viral communities. The NMDS analysis
352 showed clear differences between the NCLDV community composition of epipelagic
353 (euphotic) and mesopelagic (aphotic) zones at most sampling sites (Fig. 2B). Similar
354 results were also reported for phage communities in the Pacific Ocean[46]. The vertical
355 separation of viral communities may be caused by the stable stratification below the
356 mixed layers (typically above 200 m depth), which severely inhibits vertical water
357 exchange. Despite this limitation, mesopelagic ecosystems shared a significant number
358 (98.7%) of NCLDV phylotypes with the upper epipelagic layers (Fig. 3A), suggesting
359 the vertical connectivity of NCLDVs and their local adaptation. Indeed, some
360 mesopelagic NCLDV communities were very similar to surface communities (Fig. 6A
361 and Extended Data Fig. 7A). This implies that the surface and mesopelagic NCLDV

communities may be connected at some locations. The major source of energy and materials in the mesopelagic layer is the gravitational export of organic particles from the surface layer (i.e., the biological carbon pump)[47-49]. Therefore, some surface viruses may be exported to mesopelagic layers with sinking aggregated phytoplankton cells[50-52].

A significant positive correlation existed between surface phytoplankton biomass and NCLDV community similarity across depths (Fig. 6B and Extended Data Fig. 7B). Since highly productive areas are likely to have a greater flux of settling particles to the deep layers, this result supports the idea that NCLDVs are transported with the sinking particles. High vertical connectivity was consistently associated with an increase in NCLDV richness in the mesopelagic zone (Fig. 6C and Extended Data Fig. 7C). Previous studies showed that sinking particles can transfer bacterial and phage populations to the deep layer[52,53]. Mestre et al.[52] demonstrated that particle-attached prokaryotes had higher capacity for immigration than free-living ones. Based on the particle-driven vertical dispersion model, we can expect that NCLDVs, inside or attached to their host cells or cell debris, might be preferentially exported into the deep sea. Numerous studies based on sediment trap measurement have shown that larger phytoplankton, such as diatoms, contribute strongly to vertical flux because of their high sinking velocities[54,55]. However, recent studies show that smaller phytoplankton including haptophytes and chlorophytes, known hosts of marine NCLDVs, also contribute greatly to downward carbon export[8,9,56]. The high vertical connectivity of NCLDVs was not affected by the extent of the depth range nor by proxies for vertical mixing (Figs. 6D–F and Extended Data Figs. 7D–F), indicating that the migration of NCLDVs occurred regardless of physical processes such as upwelling, turbulent mixing, and convection. This result suggests that sinking export is a major source of a variety of NCLDVs to deeper waters, where NCLDV diversity is relatively low without this effect. A recent study revealed that some *Phycodnaviridae* and *Mimiviridae* potentially accelerate biological carbon export from the productive surface layer to deep layers, presumably by promoting cell death and aggregation of their host species[57].

390 *Phycodnaviridae* and *Mimiviridae* also contributed strongly to high vertical connectivity
391 in our study (Extended Data Figs. 8 and 9). The infection of the coccolithophore by the
392 *Phycodnaviridae* EhV was observed to facilitate the sinking of host cells, likely by
393 enhancing the production of transparent exopolymer particles and subsequent
394 aggregation[9]. Therefore, the high vertical connectivity of NCLDVs detected in our
395 analysis may be partly associated with enhanced vertical export of their infected hosts.
396 The present study expands our knowledge of marine NCLDV biogeography. Most
397 NCLDV phylotypes are ubiquitously distributed over the oceans of the globe, although
398 a high proportion of unique NCLDVs was detected in the Arctic Ocean. Our
399 comparison of community distribution patterns highlighted the tight interplay between
400 NCLDVs and microeukaryotes. As marine ecological and biogeochemical processes are
401 governed primarily by microbes, NCLDVs would have an important influence on the
402 dynamics of marine systems. We also identified unexpected similarity of NCLDV
403 communities between surface and deep waters at some locations. This supports the idea
404 that viral activity may be related to the strength of the biological carbon pump, because
405 the efficiency and sinking rate of export production depends largely on surface
406 phytoplankton composition and their infection status[8,9,55,58]. Our findings underscore the
407 importance of NCLDVs as a component of marine microbial communities, and
408 contribute to refine our knowledge of marine ecosystems, a key regulator of the Earth's
409 climate.
410

411 # Methods

412 **Sample collection**

413 Metagenomic datasets were generated from samples collected by the *Tara* Oceans
414 expeditions from 2009 to 2013[26-28,31,59]. The second version of the Ocean Microbial
415 Reference Gene Catalog (OM-RGC.v2) is a non-redundant gene catalog constructed
416 from 370 metagenomic samples from the *Tara* Oceans project[28]
417 (https://www.ocean-microbiome.org). The catalog includes 46,775,154 genes in total,

418 and the gene abundance profiles are expressed as the sum of within-reads aligned base
419 pairs normalized by gene length, in *Tara* Oceans samples[28].
420
421 **Recruitment of NCLDV marker genes from the OM-RGC.v2**
422 To assess the community composition of NCLDVs, we used family B DNA
423 polymerase (*polB*) as a marker gene of NCLDVs. Initially, amino acid sequences of the
424 OM-RGC.v2 were searched against an in-house profile hidden Markov model (HMM)
425 of NCLDV PolB sequences using the software HMMER, hmmsearch (version 3.1)[60]
426 with a threshold E-value $<1\times10^{-5}$. Consequently, 29,315 PolB sequences were obtained
427 from the OM-RGC.v2, although this collection included sequences other than NCLDVs.
428 To remove the sequences not derived from NCLDVs and classify the taxonomic identity
429 of each NCLDV sequence, phylogenetic mapping was performed within known PolB
430 sequences. A maximum-likelihood (ML) reference phylogenetic tree was built based on
431 211 PolB reference protein sequences from eukaryotes, bacteria, archaea, phages and
432 NCLDVs. These sequences were aligned using the default settings of the multiple
433 sequence alignment program MAFFT-linsi (version 7)[61] and ML tree was constructed
434 with the use of randomized axelerated maximum likelihood (RAxML) program (version
435 7.2.8)[62]. In the reference trees, we included sequences from eight proposed families of
436 NCLDVs[63]: *Mimiviridae* (synonymous with *Megaviridae*), *Phycodnaviridae*,
437 *Pithoviridae*, *Marseilleviridae*, *Ascoviridae*, *Iridoviridae*, *Asfarviridae*, and *Poxviridae*
438 (Extended Data Figs. 2–4). A sequence from a novel NCLDV clade *Medusavirus* was
439 also included as a reference[64]. Query sequences were aligned against the reference
440 alignment using the MAFFT 'addfragments' option, and then mapped onto the
441 reference tree using the software program pplacer[29].
442
443 **Abundance profiling of NCLDVs**
444 We used the abundance profile of NCLDV genes from the OM-RGC.v2 to evaluate
445 the relative frequency and diversity of NCLDVs. In the abundance matrix, we only

included samples from the pico-size (0.22–1.6 or 0.22–3.0 μm) and femto-size (<0.22 μm) fractions. Samples used in the analysis were from three depth ranges: the surface (2–9 m), the deep chlorophyll maximum (DCM, 15–180 m) and the mesopelagic (MES, 250–1,000 m). The sum of length-normalized PolB abundances ranged from 5.3 to 22,847.5 across samples. The samples containing low PolB abundances tended to yield lower diversity estimates (i.e., number of phylotypes and Shannon's entropy) (Extended Data Fig. 10). To avoid bias due to the low sequencing effort, samples for which the sum of length-normalized PolB abundance was less than 50 (set as a proxy for low NCLDV frequency) were removed from the analysis. The abundance matrix was then standardized by the sample with the lowest sum of length-normalized PolB abundance value. The minimum value of PolB abundance among NCLDV phylotypes in the sample having the lowest sum of length normalized PolB was set as the cutoff threshold. For each sample, NCLDV phylotypes with a length-normalized abundance of less than this threshold were treated as absent. A sample of a femto-size fraction of surface water from station 155 was also removed, because it contained only one NCLDV PolB after standardization. Consequently, our dataset was comprised of 283 samples (172 pico-fraction samples and 111 femto-fraction samples), covering 88 sampling sites. These sites were categorized into four biomes (coastal, trades, westerlies and polar biomes) according to latitude or distance from the shore, and nine oceanic regions, as defined by Longhurst[65] (Supplementary Table 1).

Phylogenetic tree construction

To construct a phylogenetic tree, the NCLDV-derived PolB sequences obtained from the OM-RGC.v2 were filtered by length (≥700 amino acid sequences) because the inclusion of short sequences yields unreliable phylogenies. Amino acid sequences from the resulting 911 genes were aligned with known NCLDV sequences using the *linsi* option from the MAFFT. The ML tree was constructed using RAxML with the use of a known NCLDV sequence tree as a backbone constraint. We confirmed the validity of

474 the pplacer family assignment for 905 out of 911 selected sequences. The remaining six
475 sequences that were incorrectly placed within the phylogenetic tree were removed. The
476 ML tree was visualized using the program iTOL[66].
477
478 **Prediction of potential chrysophyte viruses using metagenomic assembled genomes**
479 To explore the genomic contents of environmental NCLDVs, we made use of two
480 sets of metagenome-assembled genomes (MAGs) of NCLDVs (GVMAGs high and
481 medium quality[19]; MoMAGs[20]), which were generated from environmental
482 metagenomic datasets collected on global scales. Gene prediction was made for all
483 MAGs using the program GeneMarkS[67], then the predicted genes were searched using
484 BLASTP against a database that combines the NCBI Reference Sequence database
485 (RefSeq release 90) and the marine microbial eukaryote transcriptomes project
486 (MMETSP) database[68]. We identified MAGs whose genes exhibited the best hit to
487 transcripts of chrysophytes with >50% amino acid identity and >100 alignment length
488 (Supplementary Data 1). For these MAGs, we checked the redundancy between the
489 MoMAG and GVMAG datasets using average nucleotide identity of ≥95% and an
490 alignment fraction of ≥50% with FastANI (version 1.3)[69]. Although seven MAGs were
491 found to be overlapped between the two datasets (Supplementary Data 1), all of the
492 MAGs were retained for downstream analyses as these had different contig structures.
493 The chrysophyte-related genes were considered potential candidates for horizontal gene
494 transfer between chrysophytes and NCLDVs, and were BLASTP searched against the
495 RefSeq database for additional functional annotation (Supplementary Data 2). We then
496 extracted PolB sequences from the NCLDV MAGs which had a chrysophyte-related
497 gene using the HMMER hmmsearch program. These PolBs were BLASTP searched
498 against the NCLDV PolBs from the OM-RGC.v2. MAG-derived PolBs aligned with
499 over 700 amino acid sequences with >90% identity were assigned to the PolB
500 phylotypes derived from the OM-RGC.v2 (Supplementary Data 3). Phylogenetic
501 affiliations of PolB from the chrysophyte-related MAGs were confirmed using a

phylogenetic tree. To further test the credibility of our analysis, we checked other genes on the contigs that harbored the chrysophyte homologs using BLASTP against the RefSeq database (Supplementary Data 4; Extended Data Fig. 6).

Diversity analyses

Diversity and multivariate analyses were performed using the statistical software R (version 3.6.2) (https://www.r□project.org/). To evaluate the diversity of each sample, the number of NCLDVs (richness) and Shannon's entropy were assessed by the package 'vegan' (https://cran.r-project.org/web/packages/vegan). NCLDV richness among sizes and depths were compared using a Kruskal-Wallis test followed by Dunn's multiple comparison. Compositional variation among samples was assessed with a non-metric multidimensional scaling (NMDS) ordination based on Bray-Curtis dissimilarity. Statistical significance of differences among the sample groups (size, depth and biomes) was tested using a permutational multivariate analysis of variance (PERMANOVA)[70] with 9,999 permutations.

Partial Mantel test

A partial Mantel test was performed to assess the correlation between two multivariate matrices while controlling the potential effects of geographic distance (spatial autocorrelation) using the R package 'vegan'. Abundance matrices for the NCLDV and eukaryotic lineages were constructed from the integrated abundance tables, and the total abundance at each site was normalized to 1. The eukaryote abundance table was constructed based on 18S rRNA gene metabarcoding[71]. Data for NLCDVs were obtained from pico- (0.22–1.6/3.0 μm) or femto-size (<0.2 μm) fractions and for the eukaryotic community from the pico- to meso-size fraction (0.8–2,000 μm). There were 84 overlapping sampling events between pico-size NCLDVs and eukaryotic communities and 55 overlapping sampling events between femto-size NCLDVs and eukaryotic communities. All overlapping samples were derived from the surface or

DCM depth layers. Distance matrices for viruses and eukaryotes were calculated using the Bray-Curtis measure. Geographic distances among sample sites were also measured using Haversine distance and were used as a third distance matrix. Partial Mantel correlations were computed between all pairs of distance matrices of eukaryotic communities and NCLDVs with 9,999 permutations for each comparison. The false discovery rate (FDR) was computed using the Benjamini-Hochberg method[72].

Statistical test

Two-sided test was applied for all statistical tests.

Data availability

The complete sequence data of the OM-RGC.v2 and the abundance profile can be downloaded from https://www.ocean-microbiome.org. All sequences of 18S rRNA gene metabarcoding have been deposited at European Nucleotide Archive (ENA) under the BioProject ID PRJEB6610 and PRJEB9737. Environmental metadata are archived at https://doi.pangaea.de/10.1594/PANGAEA.875582. Files used for recruiting NCLDV PolB genes as well as processed abundance profiles of eukaryotes and NCLDVs with corresponding environmental data are available at the GenomeNet FTP: ftp://ftp.genome.jp/pub/db/community/tara/Biogeography/.

Code availability

Custom scripts developed for this study are available at GitHub: https://github.com/HisashiENDO/NCLDV_Biogeography.

Figure legends

Figure 1 Latitudinal patterns in NCLDV community composition. Relative contributions of NCLDV families at each depth range of (A) pico- and (B) femto-size fractions. The number of phylotypes detected in each sample is also indicated with a white circle. Sampling stations were arranged in rows from south to north, and color-coded based on biome (for a map of the sampling stations, please see Salazar et al., 2019[28]).

Figure 2 Community characteristics of NCLDVs. Non-metric multidimensional scaling (NMDS) ordination based on the NCLDV community showing results for all samples (A) and separately for pico- and femto-size fractions (B and C). Sample groups are color-coded by size fraction (A), depth (B) and biome (C). Ellipses represent 90% confidence levels for each group. All group categories are significantly different from each other as analyzed using PERMANOVA (p <0.01). Sample sizes for the test are noted in Supplementary Table 1.

Figure 3 Structural differentiation of NLCDV community across ecological zones. (A) Venn diagrams showing the numbers of shared or unique NLCDVs phylotypes across size fractions (left), depths (center) and biomes (right). (B) Map showing the number of total, unique and shared NCLDVs across nine oceanic regions. The map was drawn using the R package 'maps' (https://cran.r-project.org/web/packages/maps). (C) Relationships among sample size and total or unique NCLDVs detected in each region. Abbreviations: SO: Southern Ocean; RS: Red Sea; MS: Mediterranean Sea; NPO: North Pacific Ocean; NAO: North Atlantic Ocean; SAO: South Atlantic Ocean; SPO: South Pacific Ocean; IO: Indian Ocean; AO: Arctic Ocean.

Figure 4 Phylogenetic affiliations of environmental NCLDVs and their dispersal characteristics. Phylogenetic tree constructed from 905 long (≥700 amino acid) PolB sequences from the OM-RGC.v2 and 67 known NCLDV sequences (see also Extended Data Figs. 2–4 for details). The first six layers indicate the occurrence of NCLDVs unique to each size fraction, depth and biome. The outside layer denotes phylogenetic positions of known sequences (color code as in the legend) and the phylotypes closely related (>90% amino acid identity) to those of NCLDV MAGs having chrysophyte homologs (indicated in yellow). Abbreviations: OLPV-2: *Organic Lake phycodnavirus* 2; OLPV-1: *Organic Lake phycodnavirus* 1; CeV: *Chrysochromulina ericina* virus 1; PgV: *Phaeocystis globosa* virus 16T; HeV: *Haptolina ericina* virus RF02; PkV-2; *Prymnesium kappa* virus RF02; TetV-1: *Tetraselmis* virus 1; PoV: *Pyramimonas orientalis* virus 1; AaV: *Aureococcus anophagefferens*

593 virus BtV-01; PkV-1; *Prymnesium kappa* virus RF01; ChoanoV:
594 ChoanoVirus; CroV: *Cafeteria roenbergensis* virus BV-PW1; MpV-1:
595 *Micromonas* sp. RCC1109 virus MpV1; OlV-1: *Ostreococcus lucimarinus*
596 virus 1; Otv-1: *Ostreococcus tauri* virus 1; Otv-2: *Ostreococcus tauri* virus 2;
597 MpV-12T: *Micromonas pusilla* virus 12T: BpV-1: *Bathycoccus* sp. RCC1105
598 virus; BCV-FR483: *Paramecium bursaria Chlorella* virus FR-483; ACTV-1:
599 *Acanthocystis turfacea Chlorella* virus 1; PBCV-1: *Paramecium bursaria*
600 *Chlorella* virus 1; EhV-86: *Emiliania huxleyi* virus 86; FsV: *Feldmannia*
601 *species* virus; EsV-1: *Ectocampus siliculou* virus 1; *P. salinus*: *Pandoravirus*
602 *salinus*; *P. dulcis*: *Pandoravirus dulcis*; HaV-1: *Heterosigma akashiwo* virus
603 1.

604 **Figure 5 Associations between NCLDVs and eukaryotic communities.** (A) Partial
605 Mantel correlation coefficients (Spearman's ρ) between NCLDVs and
606 eukaryotic communities. Each plot shows the value of ρ computed based on
607 pico- (x-axis) and femto-sized (y-axis) NCLDV communities. Known
608 virus-host associations are shown as red dots. (B) Histogram and density
609 estimates showing the distribution of ρ values in known (red) and unknown
610 (gray) pairs. (C) Pairwise comparisons of the partial Mantel correlation
611 coefficients between NCLDV and eukaryotic lineages. Correlation
612 coefficients ρ >0.53 based on pico-size NCLDV communities are drawn as
613 edges. Known virus-host associations are shown in red, whereas unknown
614 associations are shown in gray.

615 **Figure 6 Vertical linkage of NCLDV communities between the surface and**
616 **mesopelagic layers.** (A) Latitudinal trend in NCLDV community similarity
617 between two depths (with the station numbers). Relationship between
618 NCLDV vertical similarity and (B) the surface chlorophyll *a* biomass, (C)
619 NCLDV richness in the mesopelagic layer, (D) sampling depth of
620 mesopelagic seawater, (E) the mixed layer depth and (F) temperature
621 difference between epipelagic and mesopelagic samples. All NCLDV data
622 were generated based on the pico-size fraction. Shaded areas represent 90%
623 confidence intervals.

624

625

References

1 Field, C. B., Behrenfeld, M. J., Randerson, J. T. & Falkowski, P. Primary production of the biosphere: integrating terrestrial and oceanic components. *Science* **281**, 237-240, doi:10.1126/science.281.5374.237 (1998).

2 Worden, A. Z. *et al.* Environmental science. Rethinking the marine carbon cycle: factoring in the multifarious lifestyles of microbes. *Science* **347**, 1257594, doi:10.1126/science.1257594 (2015).

3 Brum, J. R. & Sullivan, M. B. Rising to the challenge: accelerated pace of discovery transforms marine virology. *Nat Rev Microbiol* **13**, 147-159, doi:10.1038/nrmicro3404 (2015).

4 Selosse, M.-A., Charpin, M. & Not, F. Mixotrophy everywhere on land and in water: the grand écart hypothesis. *Ecology Letters* **20**, 246-263, doi:10.1111/ele.12714 (2017).

5 Weitz, J. S. *et al.* A multitrophic model to quantify the effects of marine viruses on microbial food webs and ecosystem processes. *Isme j* **9**, 1352-1364, doi:10.1038/ismej.2014.220 (2015).

6 Mojica, K. D., Huisman, J., Wilhelm, S. W. & Brussaard, C. P. Latitudinal variation in virus-induced mortality of phytoplankton across the North Atlantic Ocean. *Isme j* **10**, 500-513, doi:10.1038/ismej.2015.130 (2016).

7 Suttle, C. A. Marine viruses--major players in the global ecosystem. *Nat Rev Microbiol* **5**, 801-812, doi:10.1038/nrmicro1750 (2007).

8 Guidi, L. *et al.* Plankton networks driving carbon export in the oligotrophic ocean. *Nature* **532**, 465-470, doi:10.1038/nature16942 (2016).

9 Laber, C. P. *et al.* Coccolithovirus facilitation of carbon export in the North Atlantic. *Nat Microbiol* **3**, 537-547, doi:10.1038/s41564-018-0128-4 (2018).

10 Colson, P. *et al.* "Megavirales", a proposed new order for eukaryotic nucleocytoplasmic large DNA viruses. *Arch Virol* **158**, 2517-2521, doi:10.1007/s00705-013-1768-6 (2013).

11 Fischer, M. G. Giant viruses come of age. *Curr Opin Microbiol* **31**, 50-57, doi:10.1016/j.mib.2016.03.001 (2016).

12 Koonin, E. V. & Yutin, N. Evolution of the Large Nucleocytoplasmic DNA Viruses of Eukaryotes and Convergent Origins of Viral Gigantism. *Adv Virus Res* **103**, 167-202, doi:10.1016/bs.aivir.2018.09.002 (2019).

13 Monier, A., Claverie, J. M. & Ogata, H. Taxonomic distribution of large DNA viruses in the sea. *Genome Biol* **9**, R106, doi:10.1186/gb-2008-9-7-r106 (2008).

14 Hingamp, P. *et al.* Exploring nucleo-cytoplasmic large DNA viruses in Tara Oceans microbial metagenomes. *ISME J* **7**, 1678-1695, doi:10.1038/ismej.2013.59 (2013).

15 Clerissi, C. *et al.* Deep sequencing of amplified Prasinovirus and host green algal genes from an Indian Ocean transect reveals interacting trophic dependencies and new genotypes. *Environ Microbiol Rep* **7**, 979-989, doi:10.1111/1758-2229.12345 (2015).

16 Li, Y. *et al.* The Earth Is Small for "Leviathans": Long Distance Dispersal of Giant Viruses across Aquatic Environments. *Microbes Environ* **34**, 334-339, doi:10.1264/jsme2.ME19037 (2019).

17 Mihara, T. *et al.* Taxon Richness of "Megaviridae" Exceeds those of Bacteria and Archaea in the Ocean. *Microbes Environ* **33**, 162-171, doi:10.1264/jsme2.ME17203 (2018).

18 Li, Y. *et al.* Degenerate PCR Primers to Reveal the Diversity of Giant Viruses in Coastal Waters. *Viruses* **10**, 496, doi:10.3390/v10090496 (2018).

19 Schulz, F. *et al.* Giant virus diversity and host interactions through global metagenomics. *Nature*, doi:10.1038/s41586-020-1957-x (2020).

20 Moniruzzaman, M., Martinez-Gutierrez, C. A., Weinheimer, A. R. & Aylward, F. O. Dynamic genome evolution and complex virocell metabolism of globally-distributed giant viruses. *Nat Commun* **11**, 1710, doi:10.1038/s41467-020-15507-2 (2020).

682 21 Cottrell, M. T. & Suttle, C. A. Wide-spread occurrence and clonal variation in
683 viruses which cause lysis of a cosmopolitan, eukaryotic marine phytoplankter,
684 Micromonas pusilla. *Mar Ecol Prog Ser* **78** (1991).
685 22 Bratbak, G., Egge, J. K. & Heldal, M. Viral mortality of the marine alga
686 Emiliania huxleyi (Haptophyceae) and termination of algal blooms. *Marine*
687 *Ecology Progress Series* **93**, 39-48 (1993).
688 23 Kenji, T., Keizo, N., Shigeru, I. & Mineo, Y. Isolation of a virus infecting the
689 novel shellfish-killing dinoflagellate Heterocapsa circularisquama. *Aquatic*
690 *Microbial Ecology* **23**, 103-111 (2001).
691 24 Fischer, M. G., Allen, M. J., Wilson, W. H. & Suttle, C. A. Giant virus with a
692 remarkable complement of genes infects marine zooplankton. *Proc Natl Acad*
693 *Sci U S A* **107**, 19508-19513, doi:10.1073/pnas.1007615107 (2010).
694 25 Needham, D. M. *et al.* A distinct lineage of giant viruses brings a rhodopsin
695 photosystem to unicellular marine predators. *Proc Natl Acad Sci U S A* **116**,
696 20574-20583, doi:10.1073/pnas.1907517116 (2019).
697 26 Pesant, S. *et al.* Open science resources for the discovery and analysis of Tara
698 Oceans data. *Sci Data* **2**, 150023, doi:10.1038/sdata.2015.23 (2015).
699 27 Gregory, A. C. *et al.* Marine DNA Viral Macro- and Microdiversity from Pole to
700 Pole. *Cell* **177**, 1109-1123 e1114, doi:10.1016/j.cell.2019.03.040 (2019).
701 28 Salazar, G. *et al.* Gene Expression Changes and Community Turnover
702 Differentially Shape the Global Ocean Metatranscriptome. *Cell* **179**, 1068-1083
703 e1021, doi:10.1016/j.cell.2019.10.014 (2019).
704 29 Matsen, F. A., Kodner, R. B. & Armbrust, E. V. pplacer: linear time
705 maximum-likelihood and Bayesian phylogenetic placement of sequences onto a
706 fixed reference tree. *BMC Bioinformatics* **11**, 538,
707 doi:10.1186/1471-2105-11-538 (2010).
708 30 Gallot-Lavallee, L., Blanc, G. & Claverie, J. M. Comparative Genomics of
709 Chrysochromulina Ericina Virus and Other Microalga-Infecting Large DNA

Viruses Highlights Their Intricate Evolutionary Relationship with the Established Mimiviridae Family. *J Virol* **91**, doi:10.1128/jvi.00230-17 (2017).

31 Ibarbalz, F. M. *et al.* Global Trends in Marine Plankton Diversity across Kingdoms of Life. *Cell* **179**, 1084-1097 e1021, doi:10.1016/j.cell.2019.10.008 (2019).

32 Mihara, T. *et al.* Linking Virus Genomes with Host Taxonomy. *Viruses* **8**, 66, doi:10.3390/v8030066 (2016).

33 Ogata, H. *et al.* Remarkable sequence similarity between the dinoflagellate-infecting marine girus and the terrestrial pathogen African swine fever virus. *Virol J* **6**, 178, doi:10.1186/1743-422X-6-178 (2009).

34 Andreani, J. *et al.* Pacmanvirus, a New Giant Icosahedral Virus at the Crossroads between Asfarviridae and Faustoviruses. *J Virol* **91**, doi:10.1128/JVI.00212-17 (2017).

35 Barton, A. D., Dutkiewicz, S., Flierl, G., Bragg, J. & Follows, M. J. Patterns of diversity in marine phytoplankton. *Science* **327**, 1509-1511, doi:10.1126/science.1184961 (2010).

36 Lima-Mendez, G. *et al.* Ocean plankton. Determinants of community structure in the global plankton interactome. *Science* **348**, 1262073, doi:10.1126/science.1262073 (2015).

37 Zhou, J. & Ning, D. Stochastic Community Assembly: Does It Matter in Microbial Ecology? *Microbiol Mol Biol Rev* **81**, doi:10.1128/mmbr.00002-17 (2017).

38 Chow, C. E. & Suttle, C. A. Biogeography of Viruses in the Sea. *Annu Rev Virol* **2**, 41-66, doi:10.1146/annurev-virology-031413-085540 (2015).

39 Yoshida, T. *et al.* Locality and diel cycling of viral production revealed by a 24 h time course cross-omics analysis in a coastal region of Japan. *Isme j* **12**, 1287-1295, doi:10.1038/s41396-018-0052-x (2018).

40 Sunagawa, S. *et al.* Ocean plankton. Structure and function of the global ocean

738 microbiome. *Science* **348**, 1261359, doi:10.1126/science.1261359 (2015).
739 41 Syed, T. H., Famiglietti, J. S., Zlotnicki, V. & Rodell, M. Contemporary
740 estimates of Pan-Arctic freshwater discharge from GRACE and reanalysis.
741 *Geophysical Research Letters* **34**, doi:10.1029/2007gl031254 (2007).
742 42 Wommack, K. E. & Colwell, R. R. Virioplankton: viruses in aquatic ecosystems.
743 *Microbiol Mol Biol Rev* **64**, 69-114, doi:10.1128/mmbr.64.1.69-114.2000 (2000).
744 43 Bellec, L. *et al.* Cophylogenetic interactions between marine viruses and
745 eukaryotic picophytoplankton. *BMC Evol Biol* **14**, 59,
746 doi:10.1186/1471-2148-14-59 (2014).
747 44 Brussaard, C. P. D., Kempers, R. S., Kop, A. J., Riegman, R. & Heldal, M.
748 Virus-like particles in a summer bloom of Emiliania huxleyi in the North Sea.
749 *Aquatic Microbial Ecology* **10**, 105-113 (1996).
750 45 Stephan, J. *et al.* Flow cytometric analysis of an Emiliana huxleyi bloom
751 terminated by viral infection. *Aquatic Microbial Ecology* **27**, 111-124 (2002).
752 46 Hurwitz, B. L., Westveld, A. H., Brum, J. R. & Sullivan, M. B. Modeling
753 ecological drivers in marine viral communities using comparative metagenomics
754 and network analyses. *Proc Natl Acad Sci U S A* **111**, 10714-10719,
755 doi:10.1073/pnas.1319778111 (2014).
756 47 Herndl, G. J. & Reinthaler, T. Microbial control of the dark end of the biological
757 pump. *Nat Geosci* **6**, 718-724, doi:10.1038/ngeo1921 (2013).
758 48 Giering, S. L. *et al.* Reconciliation of the carbon budget in the ocean's twilight
759 zone. *Nature* **507**, 480-483, doi:10.1038/nature13123 (2014).
760 49 Boyd, P. W., Claustre, H., Levy, M., Siegel, D. A. & Weber, T. Multi-faceted
761 particle pumps drive carbon sequestration in the ocean. *Nature* **568**, 327-335,
762 doi:10.1038/s41586-019-1098-2 (2019).
763 50 Janice, E. L. & Curtis, A. S. Effect of viral infection on sinking rates of
764 Heterosigma akashiwo and its implications for bloom termination. *Aquatic*
765 *Microbial Ecology* **37**, 1-7 (2004).

766 51 Close, H. G. *et al.* Export of submicron particulate organic matter to
767 mesopelagic depth in an oligotrophic gyre. *Proc Natl Acad Sci U S A* **110**,
768 12565-12570, doi:10.1073/pnas.1217514110 (2013).
769 52 Mestre, M. *et al.* Sinking particles promote vertical connectivity in the ocean
770 microbiome. *Proc Natl Acad Sci U S A* **115**, E6799-E6807,
771 doi:10.1073/pnas.1802470115 (2018).
772 53 Hurwitz, B. L., Brum, J. R. & Sullivan, M. B. Depth-stratified functional and
773 taxonomic niche specialization in the 'core' and 'flexible' Pacific Ocean Virome.
774 *Isme j* **9**, 472-484, doi:10.1038/ismej.2014.143 (2015).
775 54 Sancetta, C., Villareal, T. & Falkowski, P. Massive fluxes of rhizosolenid
776 diatoms: A common occurrence? *Limnology and Oceanography* **36**, 1452-1457,
777 doi:10.4319/lo.1991.36.7.1452 (1991).
778 55 Kawakami, H. & Honda, M. C. Time-series observation of POC fluxes
779 estimated from 234Th in the northwestern North Pacific. *Deep Sea Research*
780 *Part I: Oceanographic Research Papers* **54**, 1070-1090,
781 doi:10.1016/j.dsr.2007.04.005 (2007).
782 56 Richardson, T. L. & Jackson, G. A. Small phytoplankton and carbon export from
783 the surface ocean. *Science* **315**, 838-840, doi:10.1126/science.1133471 (2007).
784 57 Blanc-Mathieu, R. *et al.* Viruses of the eukaryotic plankton are predicted to
785 increase carbon export efficiency in the global sunlit ocean. *bioRxiv*, 710228,
786 doi:10.1101/710228 (2019).
787 58 Iversen, M. H. & Ploug, H. Ballast minerals and the sinking carbon flux in the
788 ocean: carbon-specific respiration rates and sinking velocity of marine snow
789 aggregates. *Biogeosciences* **7**, 2613-2624, doi:10.5194/bg-7-2613-2010 (2010).
790 59 Alberti, A. *et al.* Viral to metazoan marine plankton nucleotide sequences from
791 the Tara Oceans expedition. *Sci Data* **4**, 170093, doi:10.1038/sdata.2017.93
792 (2017).
793 60 Eddy, S. R. Profile hidden Markov models. *Bioinformatics* **14**, 755-763,

794 doi:10.1093/bioinformatics/14.9.755 (1998).
795 61 Katoh, K. & Standley, D. M. MAFFT multiple sequence alignment software
796 version 7: improvements in performance and usability. *Mol Biol Evol* **30**,
797 772-780, doi:10.1093/molbev/mst010 (2013).
798 62 Stamatakis, A. RAxML-VI-HPC: maximum likelihood-based phylogenetic
799 analyses with thousands of taxa and mixed models. *Bioinformatics* **22**,
800 2688-2690, doi:10.1093/bioinformatics/btl446 (2006).
801 63 Koonin, E. V. & Yutin, N. Multiple evolutionary origins of giant viruses.
802 *F1000Res* **7**, doi:10.12688/f1000research.16248.1 (2018).
803 64 Yoshikawa, G. *et al.* Medusavirus, a Novel Large DNA Virus Discovered from
804 Hot Spring Water. *J Virol* **93**, doi:10.1128/JVI.02130-18 (2019).
805 65 Longhurst, A. R. in *Ecological Geography of the Sea (Second Edition)* (ed
806 Alan R. Longhurst) 89-102 (Academic Press, 2007).
807 66 Letunic, I. & Bork, P. Interactive tree of life (iTOL) v3: an online tool for the
808 display and annotation of phylogenetic and other trees. *Nucleic Acids Res* **44**,
809 W242-245, doi:10.1093/nar/gkw290 (2016).
810 67 Besemer, J., Lomsadze, A. & Borodovsky, M. GeneMarkS: a self-training
811 method for prediction of gene starts in microbial genomes. Implications for
812 finding sequence motifs in regulatory regions. *Nucleic Acids Res* **29**, 2607-2618,
813 doi:10.1093/nar/29.12.2607 (2001).
814 68 Keeling, P. J. *et al.* The Marine Microbial Eukaryote Transcriptome Sequencing
815 Project (MMETSP): illuminating the functional diversity of eukaryotic life in
816 the oceans through transcriptome sequencing. *PLoS Biol* **12**, e1001889,
817 doi:10.1371/journal.pbio.1001889 (2014).
818 69 Jain, C., Rodriguez, R. L., Phillippy, A. M., Konstantinidis, K. T. & Aluru, S.
819 High throughput ANI analysis of 90K prokaryotic genomes reveals clear species
820 boundaries. *Nat Commun* **9**, 5114, doi:10.1038/s41467-018-07641-9 (2018).
821 70 Anderson, M. J. A new method for non-parametric multivariate analysis of

variance. *Austral Ecology* **26**, 32-46, doi:10.1111/j.1442-9993.2001.01070.pp.x (2001).

71 de Vargas, C. *et al.* Ocean plankton. Eukaryotic plankton diversity in the sunlit ocean. *Science* **348**, 1261605, doi:10.1126/science.1261605 (2015).

72 Benjamini, Y. & Hochberg, Y. Controlling the False Discovery Rate: A Practical and Powerful Approach to Multiple Testing. *Journal of the Royal Statistical Society: Series B (Methodological)* **57**, 289-300, doi:10.1111/j.2517-6161.1995.tb02031.x (1995).

Acknowledgement

This work was supported by JSPS/KAKENHI (Nos. 26430184, 18H02279, and 19H05667 to H.O. and Nos. 19K15895 and 19H04263 to H.E.), Scientific Research on Innovative Areas from the Ministry of Education, Culture, Science, Sports and Technology (MEXT) of Japan (Nos. 16H06429, 16K21723, and 16H06437 to H.O.), Kyoto University Research Coordination Alliance (funding to H.E.), and the Collaborative Research Program of the Institute for Chemical Research, Kyoto University (Nos. 2019-30 and 2020-27). Computational time was provided by the SuperComputer System, Institute for Chemical Research, Kyoto University. We further thank the *Tara* Oceans consortium, the projects OCEANOMICS (ANR-11-BTBR-0008) and France Genomique (ANR-10-INBS-09), and the people and sponsors who supported *Tara* Oceans. *Tara* Oceans (that includes both the *Tara* Oceans and *Tara* Oceans Polar Circle expeditions) would not exist without the leadership of the *Tara* Expeditions Foundation and the continuous support of 23 institutes (https://oceans.taraexpeditions.org). This article is contribution number 108 of *Tara* Oceans.

Author contributions

HE and HO designed the study. HE performed most of the bioinformatics analysis. RB-M and YL contributed to the bioinformatics analysis. GS, NH, KL, CdV, MBS, CB,

PW, LK-B, and SS contributed to the generation of primary data. CdV, MBS, CB, PW, LK-B, SS, and HO coordinated *Tara* Oceans. All authors contributed to the writing of the manuscript.

Materials & Correspondence

Correspondence and material requests should be addressed to HO (email: ogata@kuicr.kyoto-u.ac.jp).

Competing financial interests

The authors declare no competing financial interests.

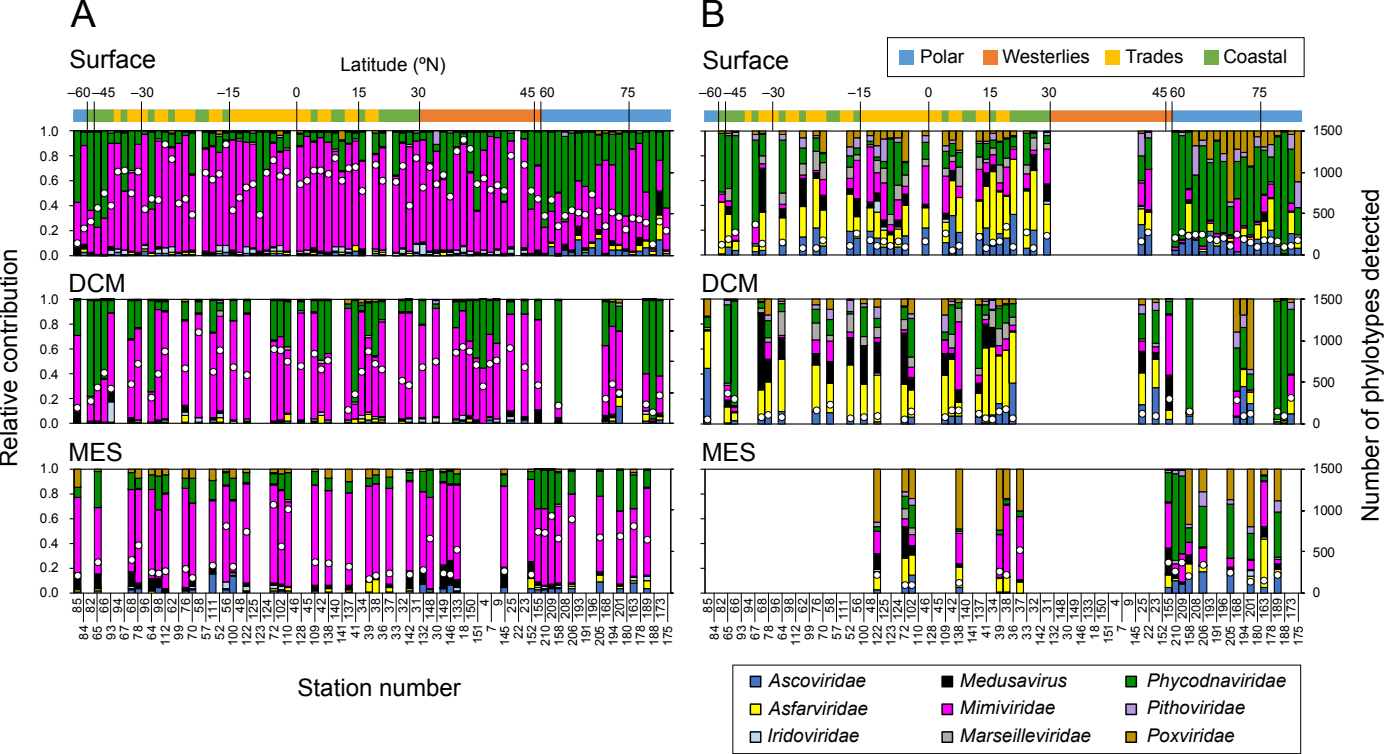
A
B
Surface
DCM
MES
Latitude (ºN)
−60 −45 −30 −15 0 15 30 45 60 75
Polar
Westerlies
Trades
Coastal
Relative contribution
Number of phylotypes detected
Station number
Ascoviridae
Asfarviridae
Iridoviridae
Medusavirus
Mimiviridae
Marseilleviridae
Phycodnaviridae
Pithoviridae
Poxviridae

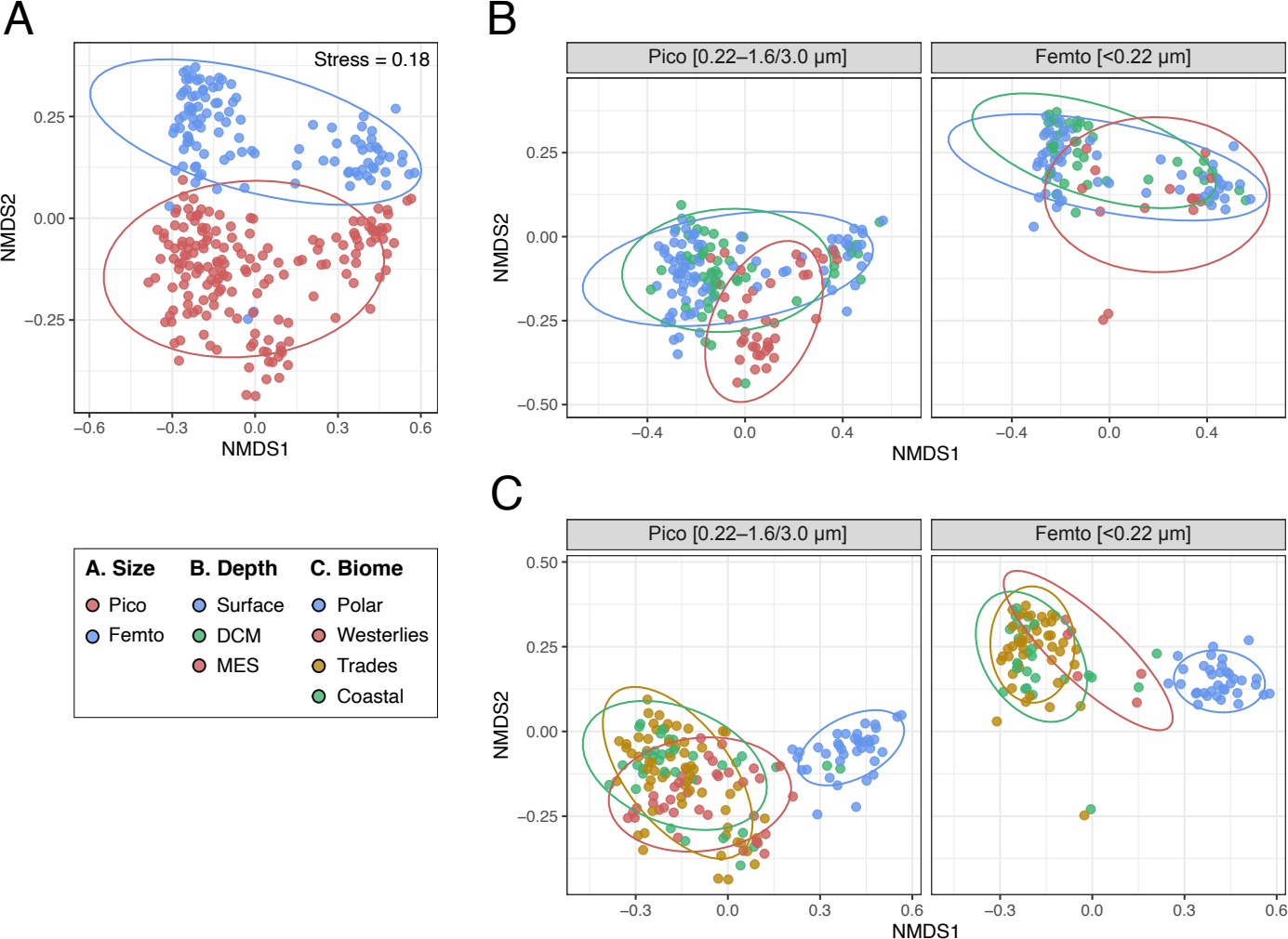
A
Stress = 0.18
NMDS2
NMDS1
B
Pico [0.22–1.6/3.0 µm]
Femto [<0.22 µm]
NMDS2
NMDS1
C
Pico [0.22–1.6/3.0 µm]
Femto [<0.22 µm]
NMDS2
NMDS1
A. Size
Pico
Femto
B. Depth
Surface
DCM
MES
C. Biome
Polar
Westerlies
Trades
Coastal

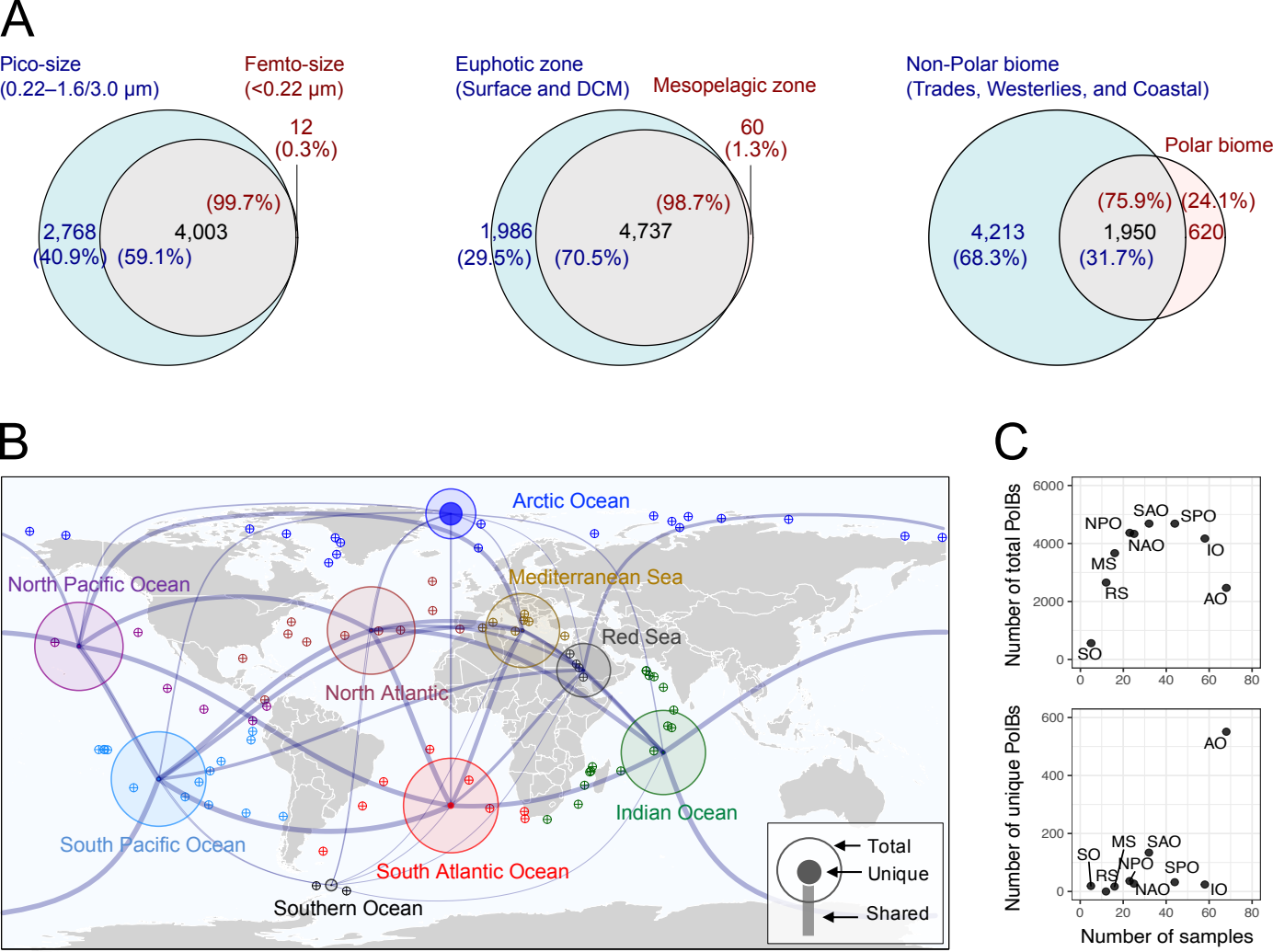
A
Pico-size
(0.22–1.6/3.0 μm)
Femto-size
(<0.22 μm)
12
(0.3%)
(99.7%)
2,768
(40.9%)
4,003
(59.1%)
Euphotic zone
(Surface and DCM)
Mesopelagic zone
60
(1.3%)
(98.7%)
1,986
(29.5%)
4,737
(70.5%)
Non-Polar biome
(Trades, Westerlies, and Coastal)
Polar biome
(75.9%)
(24.1%)
4,213
(68.3%)
1,950
(31.7%)
620
B
Arctic Ocean
North Pacific Ocean
Mediterranean Sea
Red Sea
North Atlantic
Indian Ocean
South Pacific Ocean
South Atlantic Ocean
Southern Ocean
Total
Unique
Shared
C
Number of total PolBs
NPO
SAO
SPO
NAO
IO
MS
RS
AO
SO
Number of unique PolBs
Number of samples

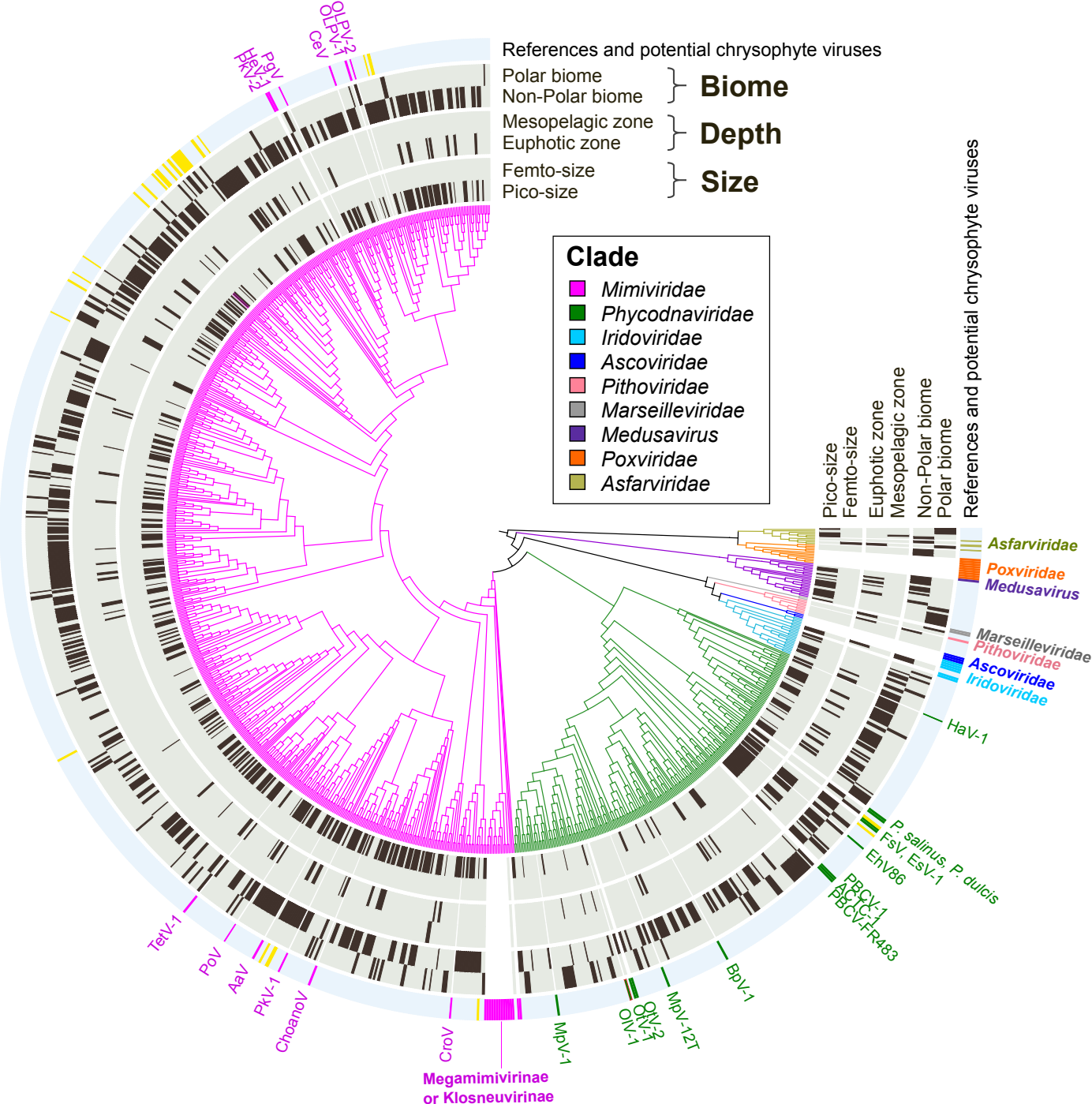
References and potential chrysophyte viruses
Polar biome
Non-Polar biome
Biome
Mesopelagic zone
Euphotic zone
Depth
Femto-size
Pico-size
Size
Clade
Mimiviridae
Phycodnaviridae
Iridoviridae
Ascoviridae
Pithoviridae
Marseilleviridae
Medusavirus
Poxviridae
Asfarviridae
Pico-size
Femto-size
Euphotic zone
Mesopelagic zone
Non-Polar biome
Polar biome
References and potential chrysophyte viruses
Asfarviridae
Poxviridae
Medusavirus
Marseilleviridae
Pithoviridae
Ascoviridae
Iridoviridae
HaV-1
P. salinus, P. dulcis
FsV, EsV-1
EhV86
PBCV-1
AR158
PBCV-FR483
BpV-1
MpV-12T
OlV-2
OlV-1
MpV-1
CroV
Megamimivirinae
or Klosneuvirinae
ChoanoV
PkV-1
AaV
PoV
TetV-1
CeV
OLPV-2
OLPV-1
HeV
PpV
PsV-1

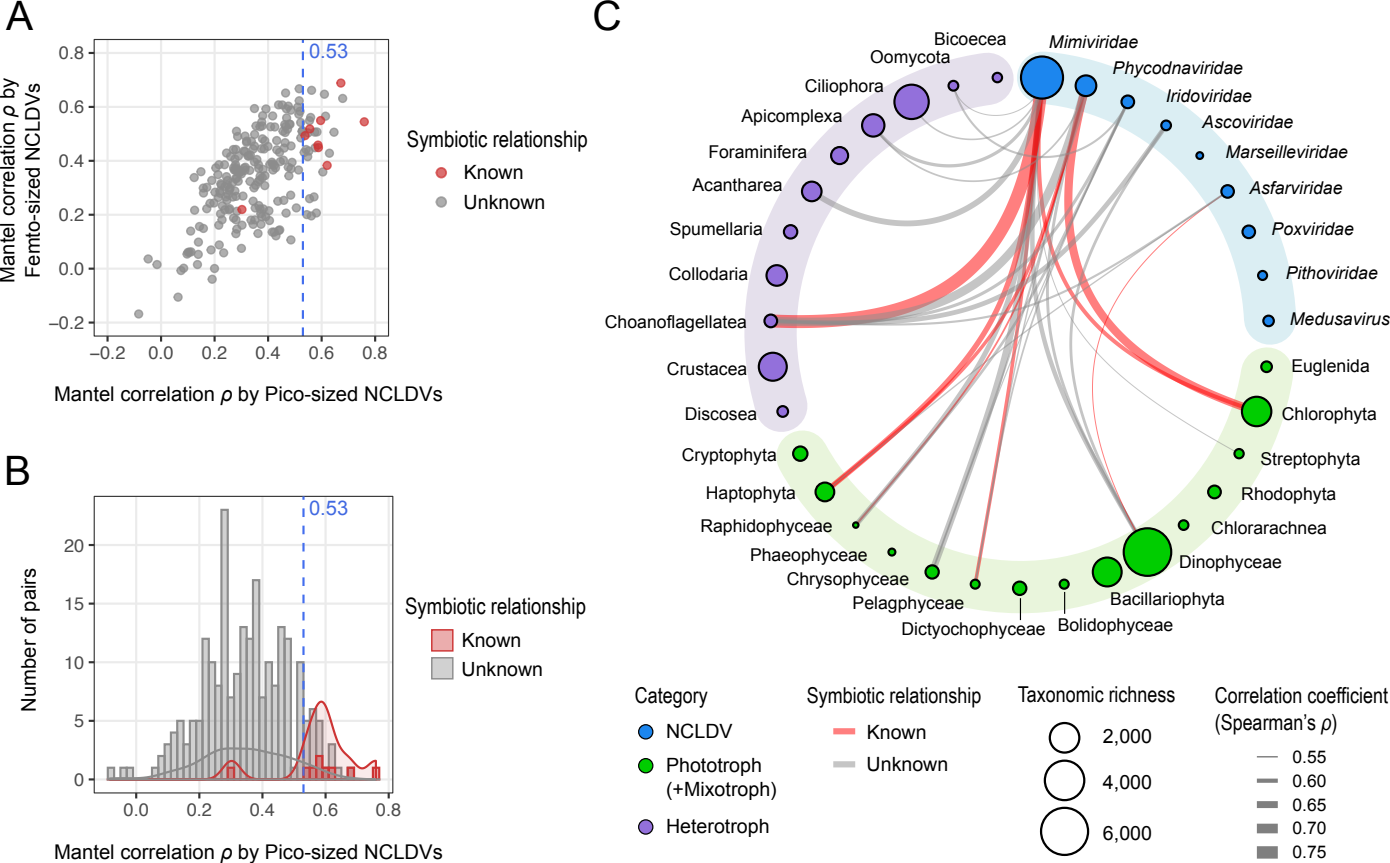
A
0.53
Mantel correlation ρ by Femto-sized NCLDVs
Mantel correlation ρ by Pico-sized NCLDVs
Symbiotic relationship
Known
Unknown
B
0.53
Number of pairs
Mantel correlation ρ by Pico-sized NCLDVs
Symbiotic relationship
Known
Unknown
C
Bicoecea
Oomycota
Ciliophora
Apicomplexa
Foraminifera
Acantharea
Spumellaria
Collodaria
Choanoflagellatea
Crustacea
Discosea
Cryptophyta
Haptophyta
Raphidophyceae
Phaeophyceae
Chrysophyceae
Pelagphyceae
Dictyochophyceae
Bolidophyceae
Bacillariophyta
Dinophyceae
Chlorarachnea
Rhodophyta
Streptophyta
Chlorophyta
Euglenida
Medusavirus
Pithoviridae
Poxviridae
Asfarviridae
Marseilleviridae
Ascoviridae
Iridoviridae
Phycodnaviridae
Mimiviridae
Category
NCLDV
Phototroph (+Mixotroph)
Heterotroph
Symbiotic relationship
Known
Unknown
Taxonomic richness
2,000
4,000
6,000
Correlation coefficient (Spearman's ρ)
0.55
0.60
0.65
0.70
0.75

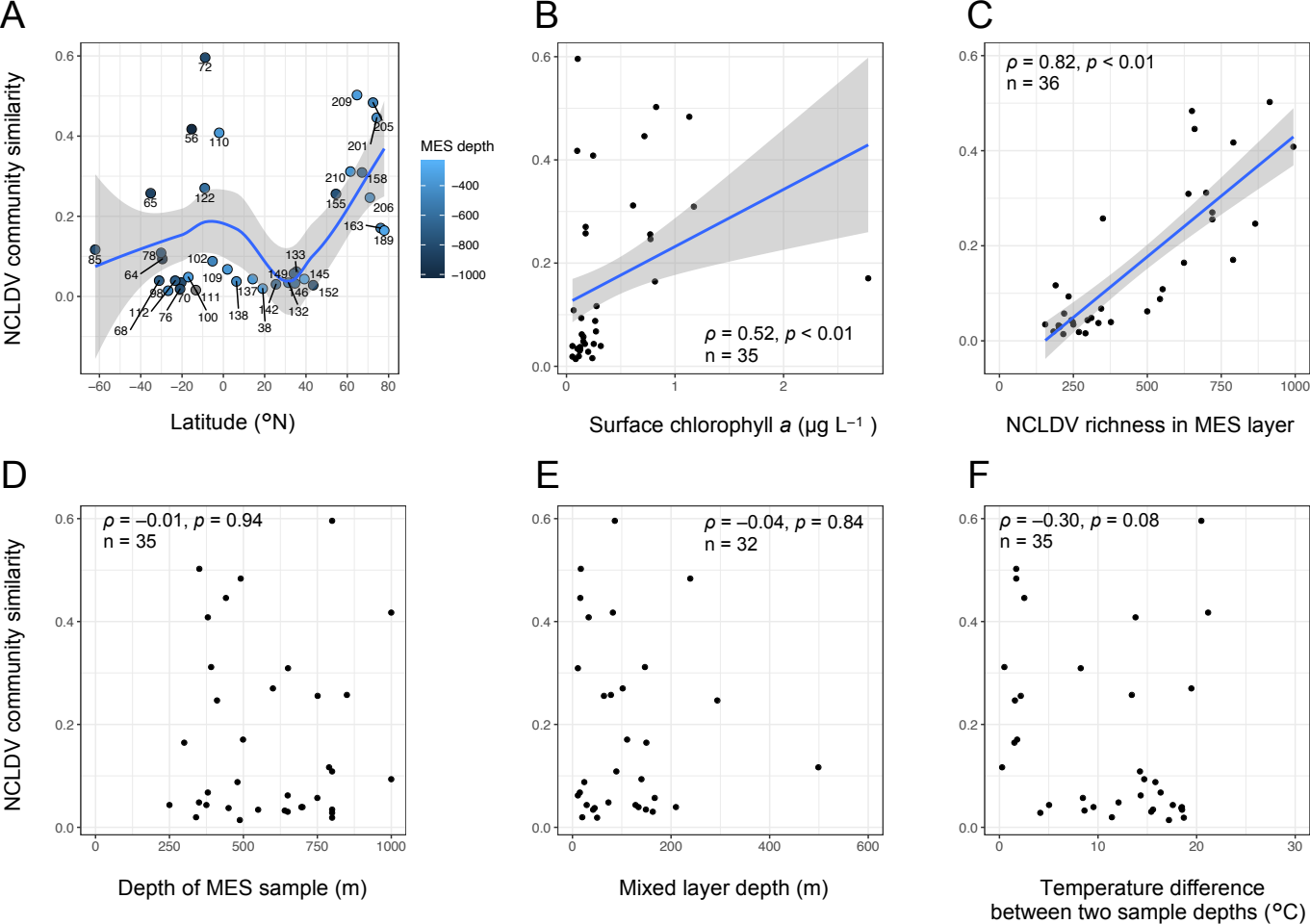
A
B
C
D
E
F
NCLDV community similarity
Latitude (°N)
MES depth
−400
−600
−800
−1000
Surface chlorophyll a (µg L⁻¹)
ρ = 0.52, p < 0.01
n = 35
ρ = 0.82, p < 0.01
n = 36
NCLDV richness in MES layer
ρ = –0.01, p = 0.94
n = 35
Depth of MES sample (m)
ρ = –0.04, p = 0.84
n = 32
Mixed layer depth (m)
ρ = –0.30, p = 0.08
n = 35
Temperature difference
between two sample depths (°C)

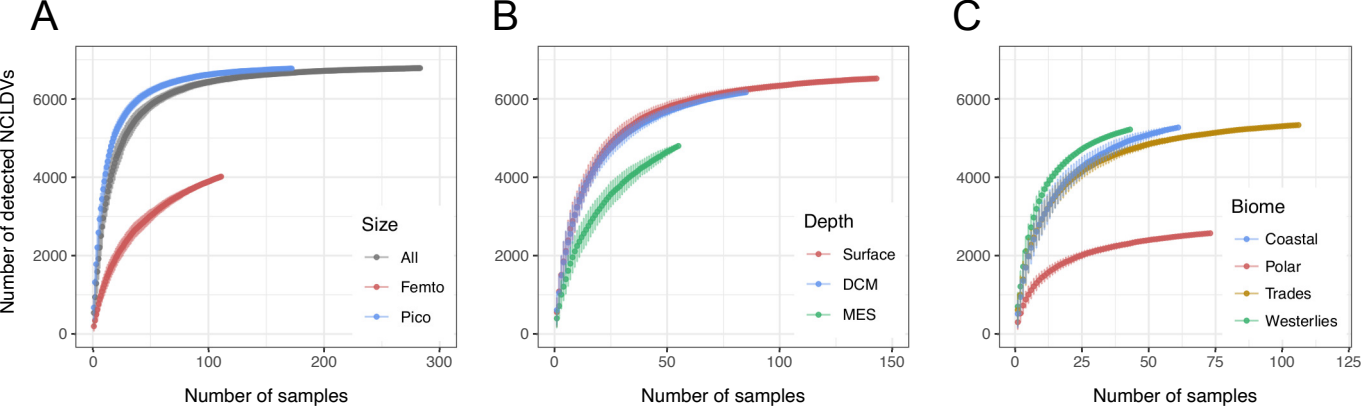
A
B
C
Number of detected NCLDVs
0
2000
4000
6000
0
100
200
300
Number of samples
Size
All
Femto
Pico
0
50
100
150
Number of samples
Depth
Surface
DCM
MES
0
25
50
75
100
125
Number of samples
Biome
Coastal
Polar
Trades
Westerlies

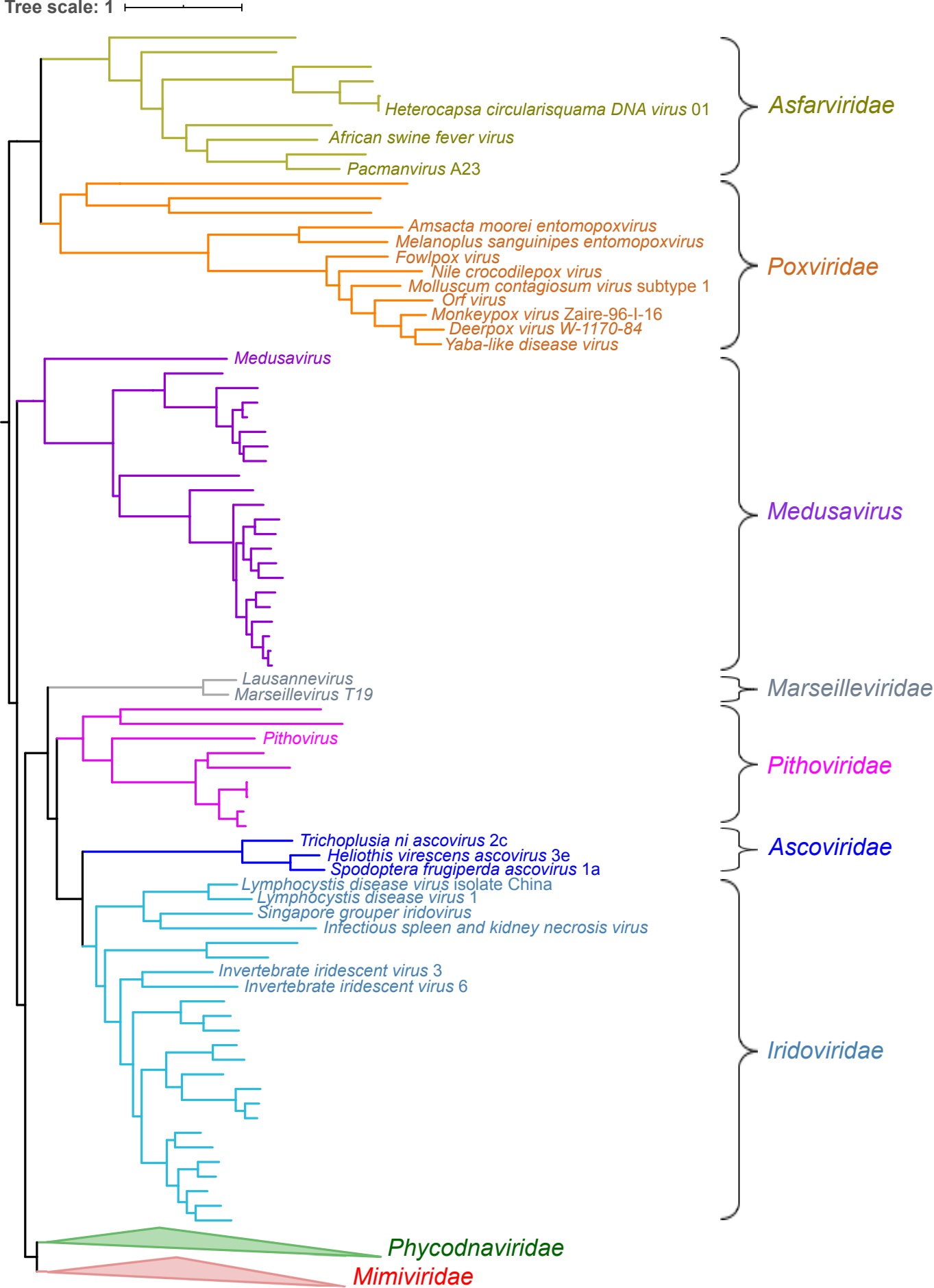
Tree scale: 1
Heterocapsa circularisquama DNA virus 01
African swine fever virus
Pacmanvirus A23
Asfarviridae
Amsacta moorei entomopoxvirus
Melanoplus sanguinipes entomopoxvirus
Fowlpox virus
Nile crocodilepox virus
Molluscum contagiosum virus subtype 1
Orf virus
Monkeypox virus Zaire-96-I-16
Deerpox virus W-1170-84
Yaba-like disease virus
Poxviridae
Medusavirus
Medusavirus
Lausannevirus
Marseillevirus T19
Marseilleviridae
Pithovirus
Pithoviridae
Trichoplusia ni ascovirus 2c
Heliothis virescens ascovirus 3e
Spodoptera frugiperda ascovirus 1a
Ascoviridae
Lymphocystis disease virus isolate China
Lymphocystis disease virus 1
Singapore grouper iridovirus
Infectious spleen and kidney necrosis virus
Invertebrate iridescent virus 3
Invertebrate iridescent virus 6
Iridoviridae
Phycodnaviridae
Mimiviridae


Tree Scale: 1
Other NCLDVs
Heterosigma akasiwo virus (HaV) 01
Pandoravirus dulcis
Pandoravirus salinus
Ectocarpus siliculosus virus1
Feldmannia species virus
ERX552279_2_dc
GVMAG-S-1016713-165
Emiliania huxleyi virus (EhV) 86
Paramecium bursaria Chlorella virus (PBCV) 1
Acanthocystis turfacea Chlorella virus (ACTV) 1
Paramecium bursaria Chlorella virus (PBCV) FR483
Bathycoccus sp. virus (BpV) RCC1105
Micromonas pusilla virus (MpV) 12T
Ostreococcus tauri virus (OtV) 2
Ostreococcus tauri virus (OtV) 1
Ostreococcus lucimarinus virus (OlV) 1
Micromonas pusilla virus (Mp V) 1
Mimiviridae


Tree Scale: 1
Other NCLDVs
Megamimivirinae or Klosneuvirinae
(Namao virus, Bodo saltans virus, Tupanvirus, Terra vrirus, Pointerouge virus, Megavirus, Acanthamoeba polyphage mimivirus, Hirudovirus strain Sangsue, Moumouvirus)
GVMAG-S-ERX555967-93
Cafeteria roenbergensis virus (CroV) VB-PW1
Choanovirus 1
Prymnesium kappa virus (PkV) RF01
ERX556015_14_dc; ERX555978_20_dc
ERX556103_23_dc
Aureococcus anophagefferens virus (AaV) BtV-01
Pyramimonas orientalis virus (PoV)1
Tetraselmis virus (TetV)1
ERX552270_36_dc
GVMAG-S-1096102-67
ERX556106_20_dc; GVMAG-S-ERX556106-38
SRX802202_64_dc; GVMAG-S-1016713-123; GVMAG-S-1074262-51
SRX802073_99_dc
ERX555943_9_dc; ERX556019_45_dc; GVMAG-S-ERX555943-30; GVMAG-S-3300000226-21
GVMAG-S-1016713-148
ERX556031_42_dc
GVMAG-M-3300021960-2, GVMAG-M-3300024314-16, ERX552270_73_dc, ERX552283_5_dc, GVMAG-M-3300024261-61, SRX802073_139_dc; GVMAG-M-3300025699-48, GVMAG-M-3300024299-4, ERX555964_34_dc, ERX555967_26_dc
Prymnesium kappa virus (PkV)RF02
Haptolina ericina virus (HeV)RF02
Phaeocystis globosa virus (PgV)16T
Chrysochromulina ericina virus (CeV)1
Organic Lake phycodnavirus (OLPV)1
Organic Lake phycodnavirus (OLPV)2
GVMAG-S-ERX555967-113

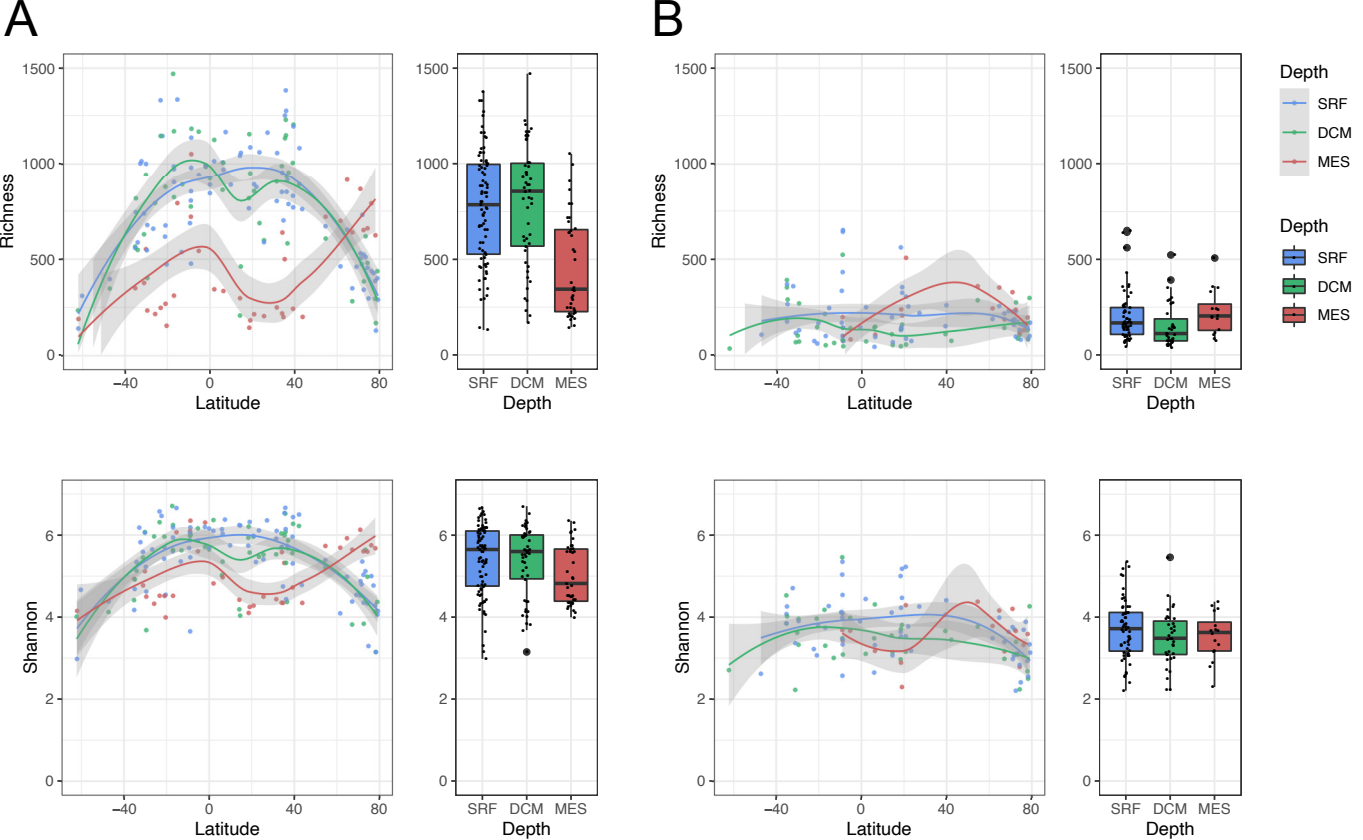
A
B
Richness
Shannon
Latitude
Depth
SRF
DCM
MES
−40
0
40
80
0
500
1000
1500
0
2
4
6

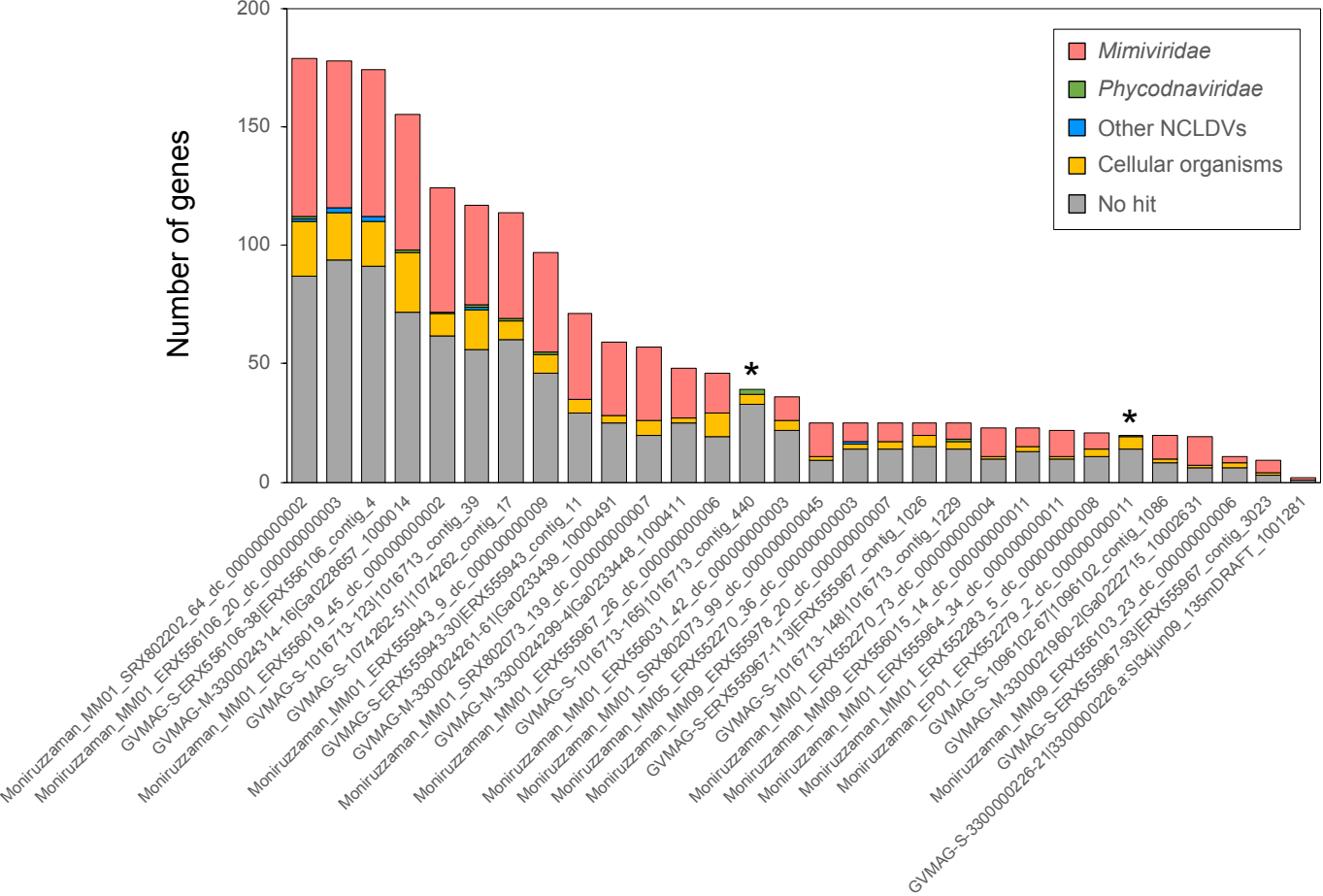
Number of genes
200
150
100
50
0
Mimiviridae
Phycodnaviridae
Other NCLDVs
Cellular organisms
No hit
*
*
Moniruzzaman_MM01_SRX802202_64_dc_000000000002
Moniruzzaman_MM01_ERX556106_20_dc_000000000003
GVMAG-S-ERX556106-38|ERX556106_contig_4
GVMAG-M-3300024314-16|Ga0228657_100014
Moniruzzaman_MM01_ERX556019_45_dc_000000000002
GVMAG-S-1016713-123|1016713_contig_39
GVMAG-S-1074262-51|1074262_contig_17
Moniruzzaman_MM01_ERX555943_9_dc_000000000009
GVMAG-S-ERX555943-30|ERX555943_contig_11
GVMAG-M-3300024261-61|Ga0233439_10000491
Moniruzzaman_MM01_SRX802073_139_dc_000000000007
GVMAG-M-3300024299-4|Ga0233448_1000411
Moniruzzaman_MM01_ERX555967_26_dc_000000000006
GVMAG-S-1016713-165|1016713_contig_440
Moniruzzaman_MM01_ERX556031_42_dc_000000000003
Moniruzzaman_MM05_SRX802073_99_dc_000000000045
GVMAG-S-ERX552270_36_dc_000000000003
GVMAG-S-ERX555978_20_dc_000000000007
GVMAG-S-1016713-113|ERX555967_contig_1026
GVMAG-S-1016713-148|1016713_contig_1229
Moniruzzaman_MM01_ERX552270_73_dc_000000000004
Moniruzzaman_MM09_ERX556015_14_dc_000000000011
Moniruzzaman_MM01_ERX555964_34_dc_000000000011
Moniruzzaman_EP01_ERX552283_5_dc_000000000008
GVMAG-S-1096102-67|1096102_contig_1086
GVMAG-M-3300021960-2|Ga0222715_10002631
Moniruzzaman_MM09_ERX556103_23_dc_000000000006
GVMAG-S-ERX555967-93|ERX555967_contig_3023
GVMAG-S-3300000226-21|3300000226.a:Sl34jun09_135mDRAFT_1001281

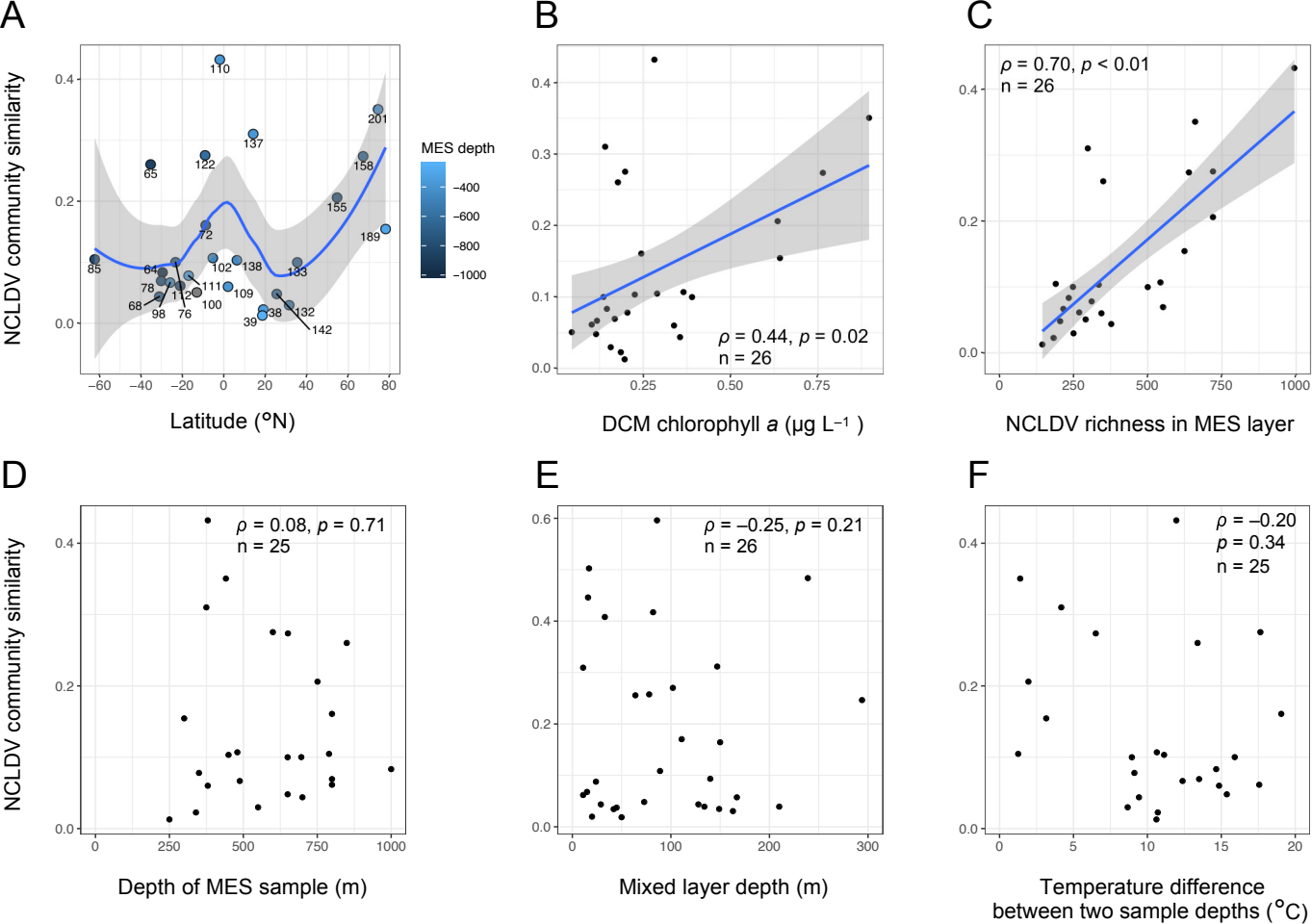
A
B
C
D
E
F
NCLDV community similarity
Latitude (°N)
MES depth
−400
−600
−800
−1000
110
201
137
65
122
158
155
72
189
85
64
102
138
133
78
111
109
112
68
100
98
76
39
38
132
142
ρ = 0.44, p = 0.02
n = 26
DCM chlorophyll a (µg L⁻¹)
ρ = 0.70, p < 0.01
n = 26
NCLDV richness in MES layer
ρ = 0.08, p = 0.71
n = 25
Depth of MES sample (m)
ρ = −0.25, p = 0.21
n = 26
Mixed layer depth (m)
ρ = −0.20
p = 0.34
n = 25
Temperature difference
between two sample depths (°C)

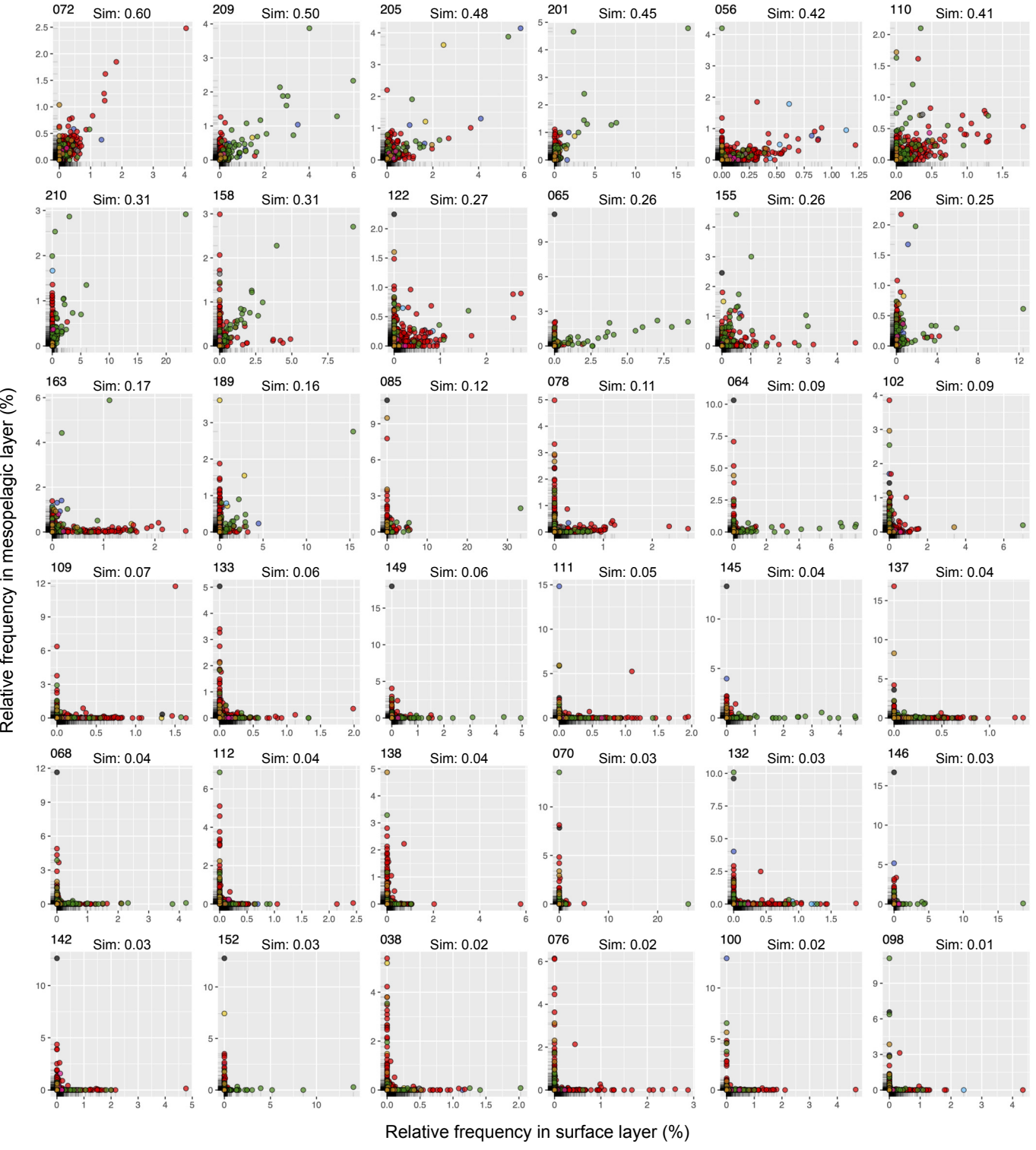
072 Sim: 0.60
209 Sim: 0.50
205 Sim: 0.48
201 Sim: 0.45
056 Sim: 0.42
110 Sim: 0.41
210 Sim: 0.31
158 Sim: 0.31
122 Sim: 0.27
065 Sim: 0.26
155 Sim: 0.26
206 Sim: 0.25
163 Sim: 0.17
189 Sim: 0.16
085 Sim: 0.12
078 Sim: 0.11
064 Sim: 0.09
102 Sim: 0.09
109 Sim: 0.07
133 Sim: 0.06
149 Sim: 0.06
111 Sim: 0.05
145 Sim: 0.04
137 Sim: 0.04
068 Sim: 0.04
112 Sim: 0.04
138 Sim: 0.04
070 Sim: 0.03
132 Sim: 0.03
146 Sim: 0.03
142 Sim: 0.03
152 Sim: 0.03
038 Sim: 0.02
076 Sim: 0.02
100 Sim: 0.02
098 Sim: 0.01
Relative frequency in mesopelagic layer (%)
Relative frequency in surface layer (%)
Family
Ascoviridae
Asfarviridae
Iridoviridae
Medusavirus
Mimiviridae
Marseilleviridae
Phycodnaviridae
Pithoviridae
Poxviridae

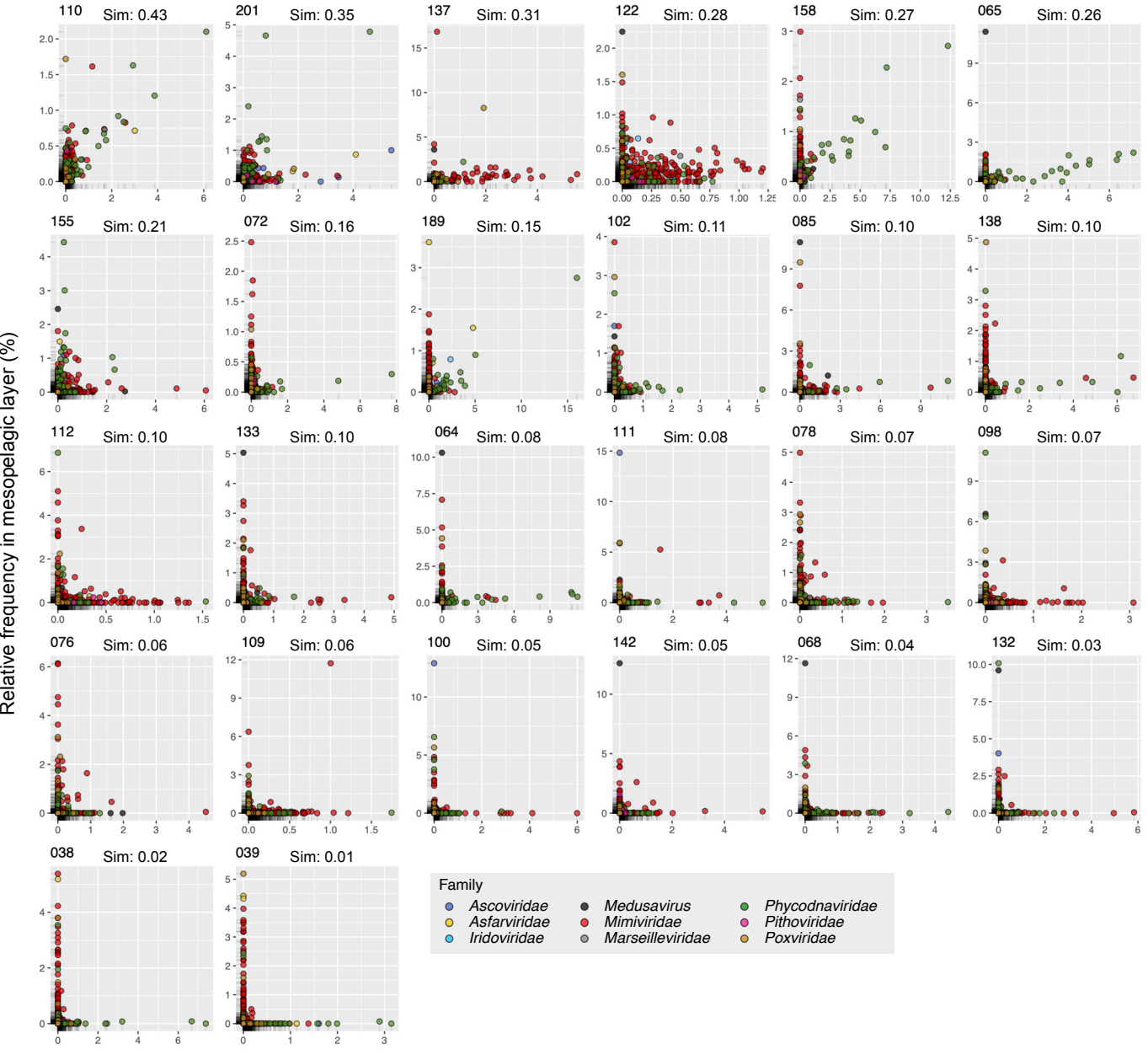
110 Sim: 0.43
201 Sim: 0.35
137 Sim: 0.31
122 Sim: 0.28
158 Sim: 0.27
065 Sim: 0.26
155 Sim: 0.21
072 Sim: 0.16
189 Sim: 0.15
102 Sim: 0.11
085 Sim: 0.10
138 Sim: 0.10
112 Sim: 0.10
133 Sim: 0.10
064 Sim: 0.08
111 Sim: 0.08
078 Sim: 0.07
098 Sim: 0.07
076 Sim: 0.06
109 Sim: 0.06
100 Sim: 0.05
142 Sim: 0.05
068 Sim: 0.04
132 Sim: 0.03
038 Sim: 0.02
039 Sim: 0.01
Family
Ascoviridae
Asfarviridae
Iridoviridae
Medusavirus
Mimiviridae
Marseilleviridae
Phycodnaviridae
Pithoviridae
Poxviridae
Relative frequency in mesopelagic layer (%)
Relative frequency in surface layer (%)

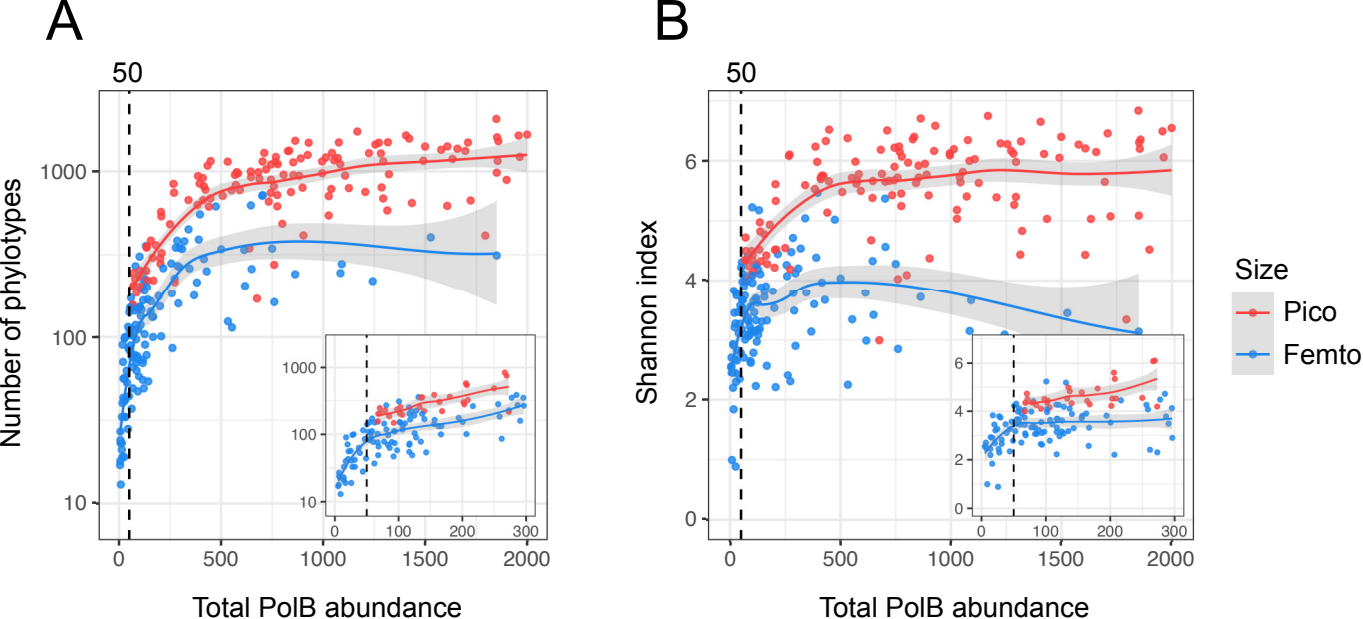
A
B
50
50
Number of phylotypes
Shannon index
Total PolB abundance
Total PolB abundance
Size
Pico
Femto
10
100
1000
0
2
4
6
0
500
1000
1500
2000
0
100
200
300